Planned Geological Investigations of the Europa Clipper Mission

I.J. Daubar[1,2] · A.G. Hayes[3] · G.C. Collins[4] · K.L. Craft[5] · J.A. Rathbun[3] · J.R. Spencer[6] · D.Y. Wyrick[7] · M.T. Bland[8] · A.G. Davies[1] · C.M. Ernst[5] · S.M. Howell[1] · E.J. Leonard[1] · A.S. McEwen[9] · J.M. Moore[10] · C.B. Phillips[1] · L.M. Prockter[5] · L.C. Quick[11] · J.E.C. Scully[1] · J.M. Soderblom[12] · S.M. Brooks[1] · M. Cable[1] · M.E. Cameron[1] · K. Chan[13] · C.J. Chivers[14] · M. Choukroun[1] · C.J. Cochrane[1] · S. Diniega[1] · A.J. Dombard[15] · C.M. Elder[1] · C. Gerekos[16] · C. Glein[7] · T.K. Greathouse[7] · C. Grima[13] · M.S. Gudipati[1] · K.P. Hand[1] · C. Hansen[17] · P. Hayne[18] · M. Hedman[19] · K. Hughson[20] · X. Jia[21] · J. Lawrence[22] · H.M. Meyer[5] · K. Miller[7] · R. Parekh[1] · G.W. Patterson[5] · D.M. Persaud[23] · S. Piqueux[1] · K.D. Retherford[7,24] · K.M. Scanlan[13] · P. Schenk[17] · B. Schmidt[25] · D. Schroeder[26] · G. Steinbrügge[1] · A. Stern[6] · G. Tobie[27] · P. Withers[28] · D.A. Young[13] · B. Buratti[1] · H. Korth[5] · D. Senske[1] · R. Pappalardo[1]

Abstract

Geological investigations planned for the Europa Clipper mission will examine the formation, evolution, and expression of geomorphic structures found on the surface. Understanding geologic features, their formation, and any recent activity are key inputs in constraining Europa's potential for habitability. In addition to providing information about the moon's habitability, the geologic study of Europa is compelling in and of itself. Here we provide a high-level, cross-instrument, and cross-discipline overview of the geologic investigations planned within the Europa Clipper mission. Europa's fascinating collection of ice-focused geology provides an unparalleled opportunity to investigate the dynamics of icy shells, ice-ocean exchange processes, and global-scale tectonic and tidal stresses. We present an overview of what is currently known about the geology of Europa, from global to local scales, highlighting outstanding issues and open questions, and detailing how the Europa Clipper mission will address them. We describe the mission's strategy for searching for and characterizing current activity in the form of possible active plumes, thermal anomalies, evidence for surface changes, and extremely fresh surface exposures. The complementary and synergistic nature of the data sets from the various instruments and their integration will be key to significantly advancing our understanding of Europa's geology.

Extended author information available on the last page of the article

1 Introduction

The presence of a likely liquid water ocean beneath the ice shell of Jupiter's moon Europa means this moon may be the most promising place in our solar system for hosting life outside of Earth (Pappalardo et al. 2024; Vance et al. 2023). Accordingly, Europa's astrobiological potential has made its exploration a priority for the three planetary decadal surveys (National Research Council 2003, 2011; National Academies of Sciences 2022). This is the primary driver behind the formulation of the Europa Clipper mission. The overall science goal of the mission is to "*Explore Europa to investigate its habitability*". However, in order to test the suitability of this ocean world for life, we must first understand its properties and the exchange processes that cycle material between the interior, ocean, icy crust, and surface. To address this goal, the mission is designed around three science objectives (Pappalardo et al. 2024):

(1) Characterize the ice shell and any subsurface water, including their heterogeneity, ocean properties, and the nature of surface-ice-ocean exchange;

(2) Understand the habitability of Europa's ocean through composition and chemistry;

(3) Understand the formation of surface features, including sites of recent or current activity; identify and characterize high science interest localities.

This paper focuses on the third of these objectives. Within the mission's science team, the Geology Thematic Working Group (GWG) focuses on investigations of formation, evolution, and expression of geomorphic structures found on Europa's surface. In addition to providing information about the moon's habitability, the geologic study of Europa is compelling in and of itself. Europa's fascinating collection of ice-focused geology provides an unparalleled opportunity to investigate the dynamics of icy shells, ice-ocean exchange processes, and global-scale tectonic responses to tidal forces.

Herein, we present an overview of what is currently known about the geology of Europa, from global (kilometers) to local (several to tens of meters) scales, highlighting outstanding issues and open questions that Europa Clipper will address. We then describe the integrated datasets that the mission will use to significantly advance our understanding of Europa's geology. The mission will revolutionize the understanding of both Europan and icy satellite geology in general and address outstanding questions such as:

- What is the global distribution, morphology, and compositional diversity of geologic landforms on Europa?
- What are the geologic processes responsible for the formation of landforms including ridges, bands, chaos terrain, smooth plains, domes, and pits? What do these formation mechanisms imply for subsurface structures, thickness and composition of the ice shell, nature of the ocean, and ice-ocean interactions?
- What do Europa's resurfacing processes imply regarding the timescales and pathways for transporting material to and from the subsurface ocean?
- Are apparent regional variations in spatial distributions of geologic features, including impact craters, real or a product of limited resolution of previous data?
- What are the relative ages of Europa's surface units? Have resurfacing processes acted globally or regionally, and are they ongoing or sporadic? Are there as yet undiscovered older terrains on Europa's surface?
- What is the nature of the surface at the meter-scale? What are the morphologic, thermophysical, and mechanical properties of the uppermost layer of Europa? How do these surface properties vary across the globe?
- Are plumes present at Europa, and if so, what is their nature - density, frequency, composition, driving mechanisms, and sources?

- What, if any, evidence is there for other current or recent geologic activity? If found, what does that tell us about resurfacing processes and rates, material properties of the regolith, and exchange with the subsurface?

The Europa Clipper mission's Thematic Working Groups (TWGs) are stewards of the mission's overall Science Goal (assess Habitability) and three Science Objectives (characterize Interior, Composition, and Geology) (Pappalardo et al. 2024). The primary goal of the GWG is to provide a high-level, cross-instrument and cross-discipline, geology-driven science perspective to these overarching objectives. Activities related to the science and safety of a future landed mission (Sect. 5) are shepherded by the Reconnaissance Focus Group (Phillips et al. 2023), which reports to the GWG. Plume search and characterization (Sect. 3.2), which are cross disciplinary activities, are shepherded by a Plume Focus Group that interacts with all four TWGs.

The GWG helps ensure that the Europa Clipper mission can meet its mission objective to understand the formation of surface features, including sites of recent or current activity, and characterize localities of high science interest. This includes oversight of the three geology-focused Level 1 requirements (Table 1), along with the geologic aspects of a cross-cutting Recent Activity theme (Pappalardo et al. 2024). These Level 1 requirements define the specific measurements that Europa Clipper must perform to complete the mission objectives; these then flow down to lower-level requirements that detail the implementation of how that science will be achieved. The mission's geology-focused Level 1 and Level 2 requirements (Table 1; supplemental information) are drawn from previous Science Definition Team reports and decadal studies (National Research Council 2003, 2011; National Academies of Sciences 2022), and are influenced by the mission's selected instrument investigation proposals to NASA.

The geology-focused science mission requirements are generally grouped by the spatial scale of the processes involved (Table 1). Global-scale data will be used to define the distribution of geologic landforms, characterize Europa's overall shape, and ultimately help to determine the thicknesses of the ice shell, ocean, and the overall subsurface structure (Roberts et al. 2023). Regional-scale data (100 s of meter scale) will be used to derive the composition (Becker et al. 2024), spatial distribution, and formation mechanisms of observed landforms, as well as characterize the near-subsurface structure and search for any perched liquid deposits. Local-scale data (less than a meter to tens of meters) will be used to determine regolith properties and characterize erosional and depositional processes operating at the meter-scale. The local- and regional-scale data will also satisfy reconnaissance objectives for future landed missions (Phillips et al. 2023).

This manuscript is organized in a parallel structure to the requirements, discussing Europa's geological processes at the global (Sect. 2.1), regional (Sect. 2.2), and local (Sect. 2.3) scales. Plumes, thermal anomalies, and other potential evidence for current surface activity are discussed in Sect. 3. In Sect. 4, we summarize the synergy between the expected datasets from all of the investigations. While these data are described in more detail the investigation papers in this collection, Sect. 4 presents a cross-instrument perspective on how the datasets are combined and complement each other to address the mission's geology-focused science objectives. Finally, planned efforts to gather reconnaissance data for a future lander, which is complementary to this mission's geology objectives and uses many of the same integrated datasets, are discussed in Sect. 5.

In addition to formal requirements that flow down from the high-level science objectives (Table 1), the Europa Clipper team also has less formal metrics referred to as "Planning Guidelines" to evaluate the scientific effectiveness of various Jupiter tours and observation plans. One Planning Guideline developed by the GWG is meant to ensure the opportunity

Table 1 High-level geology-relevant Level 1 requirements and summaries of Level 2 science requirements for the Europa Clipper mission. For full official text, see supplemental information.

Theme	Level 1 Requirements	Level 2 Requirements Summary
Geology	**Global Photomosaic:** Produce a controlled photomosaic map of ≥80% of the surface at ≤100-m spatial scale.	Characterize visible reflectance, morphology, and albedo of ≥80% of the surface at ≤100-m pixel scale to characterize structures, surface units, and the potential for shallow subsurface water.
	Landform Geology: Characterize the surface at ≤25-m spatial scale across ≥5% of the surface with global distribution, including measurements of topography at ≤15-m vertical precision across ≥1% of Europa's surface.	Characterize distribution, morphology and formation of landforms, including color imaging of ≥5% of the surface at ≤25 m/pixel, stereo imaging of ≥1% of the surface at ≤100 m/pixel.
		Sample compositionally diagnostic properties of ≥14 globally distributed sites at ≤50-m pixel scale, in order to determine composition of individual landforms, to investigate how composition influences the formation and evolution of landforms.
	Local-Scale Properties: Characterize the surface at ~1-m spatial scale to determine surface properties, for ≥18 globally distributed sites.	Characterize visible reflectance, morphology, and albedo of ≥18 sites at ~1-m/pixel, with associated topographic coverage, in order to determine regolith cohesiveness, thickness, and subsurface layering; surface roughness and slopes; and the distribution of blocks.
		Characterize visible reflectance, morphology, albedo, and color of globally distributed sites at ≤10-m/pixel, in order to characterize resurfacing and degradation by processes such as weathering and erosion as context for interpreting the local-scale imaging dataset.
		Map daytime or nighttime temperatures of ≥40 geologically distinct sites at a ≤250-m pixel scale to characterize thermophysical properties indicative of erosion and deposition processes.
		Acquire near-surface reflectometry and altimetry measurements to determine regolith cohesiveness, thickness, and subsurface layering; surface roughness and slopes; and the distribution of blocks.
Current Activity	Search for and characterize any current activity, notably plumes or thermal anomalies, in regions that are globally distributed.	Search for active plumes in limb and terminator images at high phase angle at ≤10-km pixel across a range of longitudes and true anomalies.
		Search for and characterize the vapor compositions of plumes ≥30 km in height.
		Identify any thermal anomalies at scales ≤25 m/pixel.
		Search for albedo or color changes at scales ≤500 m/pixel as compared to Voyager, Galileo, or other Europa Clipper data.
		Identify and characterize composition, density, and size of particles in any encountered plumes, constrain the source mechanism and salinity.
		Measure the composition of volatiles to determine the relative fluxes of endogenous particles and gases in any encountered plume material.
Correlation	The following datasets shall permit cross-correlation including and among each of the following categories: (1) in-situ-mapping and remote sensing datasets; (2) fields and particles (excluding gravity), and plasma plus auroral datasets, and; (3) gravity and any tidal deformation datasets.	

for simultaneous observations from all instruments over certain landforms (regional-scale geologic features), which the GWG has determined are of high scientific value. This evaluation was based on previous data showing anomalous albedo, texture, or size that indicates the landform could be particularly young or indicative of ice-shell properties. We have defined two categories of landforms, shown in Fig. 1c that are deemed to be type examples of key terrain types. Category A contains those for which it is highly desirable to have a flyby that is able to view at least one of each landform type, with all instruments taking data. Only a select number of landforms have been identified to be in this category. Category B contains landforms that the GWG assessed would benefit from having as many flybys that can view these landforms as possible while allowing all instruments the opportunity to observe simultaneously. Altitude ranges for these flybys are derived from a combination of the best observing conditions for remote sensing and in-situ instruments, and imaging instruments for which the balance between the best pixel scale/resolution and field of view are functions of altitude. (See Supplemental Information for the full text and rationale of the GWG Planning Guideline.)

2 Geologic science at different scales

Previous data have shown Europa to be a fascinating body, even at low resolution. The earliest data revealing Europa at the global scale were provided by the Voyager missions (1979), with limited spatial coverage, ranging from ∼2 km/pixel to >20 km/pixel (Lucchitta and Soderblom, 1982). The Galileo mission (1997–2003) provided an improved image data set with one image having a resolution as good as 6 m/pixel (Greeley et al. 2000). However, the high-resolution (<50 m/pixel) images were only acquired in a few limited areas, covering less than 0.03% of the total surface. Lower resolution image data, ∼1 to 2 km/pixel, cover a significant portion (∼70%) of Europa's surface and have revealed a number of unique and interconnecting landforms across its surface (e.g., Doggett et al. 2009). Perhaps the most useful Galileo imaging data for geological investigations averages approximately 250 m/pixel and covers 10% of the surface. These data include two nearly pole-to-pole mosaics separated by 120° in longitude. These mosaics have allowed many landforms to be characterized at different scales and across many latitudes, resulting in a basic understanding of Europa's general stratigraphic sequence (Figueredo and Greeley 2000, 2004). A small amount of Galileo Near-Infrared Mapping Spectrometer (NIMS) data corresponding to some of the imaged areas has yielded further information about the formation processes and evolution of some of Europa's geological features (e.g., Shirley et al. 2010; Dalton et al. 2012). Global-scale photometric and ground-based radar studies of Europa have allowed for deductions about the material properties of the surface such as roughness and porosity (e.g., review in Moore et al. 2009), but current models have many assumptions, and the data are severely limited in resolution. Thermal measurements from the Voyager and Galileo spacecraft are limited in coverage and spatial resolution, but have yielded some information about thermal inertia and heat flow (e.g., Hanel et al. 1979; Spencer 1987; Spencer et al. 1999).

Based on these limited data, we have gained substantial expertise about the array of geologic features and have formulated hypotheses regarding the processes that have shaped this unique body. Here, we briefly summarize the current state of knowledge about Europa's geology, from the global to the local scale, and discuss how the Europa Clipper mission will address the many as-yet-unanswered questions and test various hypotheses regarding geologic feature formation and evolution.

2.1 Global-scale processes

Europa's crust is affected by a combination of exogenic and endogenic processes that affect its albedo, rheological properties, and composition. Dominant exogenic processes on Europa include impact cratering and charged particle bombardment from Jupiter's radiation belts resulting in sputtering. The decameter-scale surface reveals few large (>20 km diameter) impact craters. It is instead dominated by large areas of chaos terrain and numerous ridges and bands, which can extend thousands of kilometers across surface and give Europa its unique "ball of string" appearance at the global scale (Fig. 1). Endogenic processes, including volcanism and tectonism, drive the erasure of most impact craters and the formation of those surface features.

To better lead our discussion of the geology of Europa, we begin here by defining reference systems, as these are important in understanding the interaction of the greater jovian environment and the surface. The coordinate system used here is planetocentric positive east longitude, and the longitude reference point is the center of the crater Cilix, at 178°E (Phillips and Korth 2017). (For more discussion of coordinate systems, see Sect. 4.) Europa's global geography is often described by referencing a system of overlapping hemispheres that form unique quadrants: sub-Jovian (Jupiter-facing), anti-Jovian (facing away from Jupiter), leading (facing the direction of orbital motion), and trailing (facing away from the direction of motion). The locations of the hemispheres are fixed with respect to Jupiter, as Europa is tidally locked to the planet. Dividing the surface by these four faces, each consisting of half the moon, results in four longitudinal quadrants with each defined by a unique combination of the two halves described above: trailing sub-Jovian (0°–90°E), trailing anti-Jovian (90°–180°E), leading anti-Jovian (180°–270°E), and leading sub-Jovian (270°–360°E) (Fig. 1).

2.1.1 Hemispherical Differences

There are hemispherical large-scale differences in albedo, composition, and geomorphology between Europa's four longitudinal quadrants. These can arise from exogenic processes such as implanted material from volcanic eruptions on Io, charged particle bombardment from Jupiter's radiation belts, or impactor variability (Johnson and Pilcher 1977). For synchronously rotating satellites, cratering rates, impact gardening, and micrometeorite bombardment are expected to be greater on the leading hemisphere (Zahnle et al. 2003), while plasma implantation and bombardment by high-energy electrons, protons, and heavy ions from Jupiter's radiation environment are expected to be strongest on the trailing hemisphere (Paranicas et al. 2001, 2010; Breer et al. 2019; Meitzler et al. 2023). The limited mapping coverage currently available for Europa does not permit a statistically significant determination of whether the crater density is hemispherically asymmetric (Schenk et al. 2004; Bierhaus et al. 2009). The Voyager and Galileo datasets are similarly insufficient to determine if there are hemispherical differences in albedo and color correlations driven by generation of radiolytic products (Paranicas et al. 2001, 2010; Breer et al. 2019). By determining the crater distribution (Sect. 2.2.3) and identifying materials on the surface that were likely deposited or modified as a result of high-energy electron and ion bombardment, the Europa Clipper mission will test whether nonsynchronous rotation is fast enough to erase the expected hemispherical signals (Roberts et al. 2023).

2.1.2 Ages of surfaces

Europa's surface appears to be extremely young due to the paucity of impact craters. The globally averaged surface crater retention age has been estimated to be between 40–90 Myr
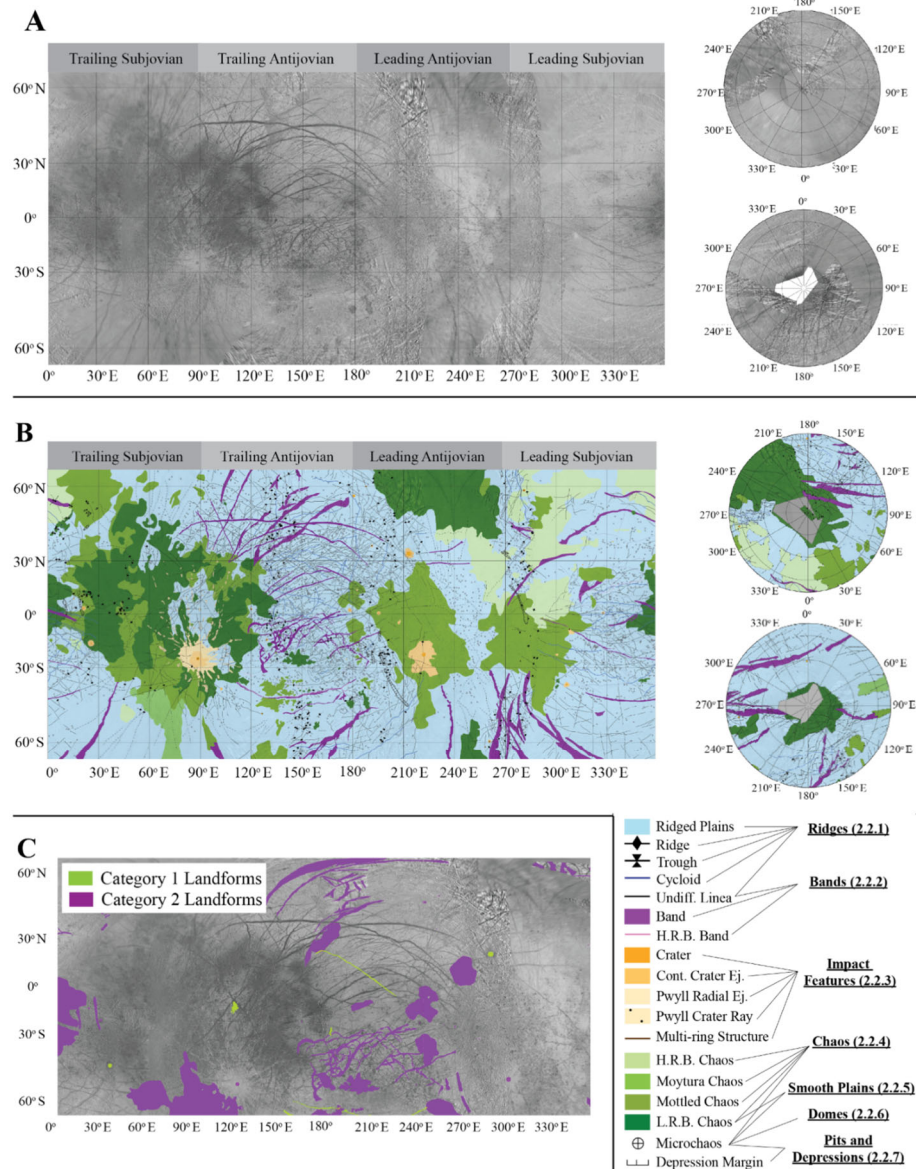
Fig. 1 (A) Global image mosaic of Europa (USGS, 2002) in east positive coordinates and simple cylindrical projection; (B) Global geologic map of Europa at 1:15M (Leonard et al. 2023). The legend for the global geologic units (lower right) is mapped to the regional geology discussed in this manuscript. (C) Combined landform map for the Europa Clipper Geology Working Group Planning Guideline (includes Bands, Chaos, Craters, and Depression landform maps). See text (Sect. 1 and supplemental material) for the definition of the categories. For examples of the features mapped here, see Fig. 2.

(e.g., Zahnle et al. 2003; Bierhaus et al. 2005, 2009; Schenk and Turtle 2009). Uncertainty in the impact rate and the mechanics of cratering in ice could expand that range to 20–200

Myr (Sect. 2.2.3). As such, obtaining a clear understanding of the distribution of impact craters is important to better constrain an average surface age.

Due to the relative lack of large primary impact craters on Europa's surface (Moore et al. 2001; Leonard et al. 2018a,b), traditional methods of relative dating of planetary surfaces using crater counts are challenging to apply on Europa. Instead, relative ages of terrains are determined using cross-cutting relations between different geologic units and relative albedos (changes in albedo as a function of time). In terms of albedo, the youngest features have been observed to have the lowest albedo (e.g., Greeley et al. 2000; Prockter et al. 2002) and many non-impact related features appear to brighten with age. It is not known whether this is due to radiation processing, micrometeorite bombardment, or changes in composition. Stratigraphic relations suggest that there have been at least three episodes of resurfacing over the visible surface history, each dominated by a different type of surface feature. The oldest period involved the formation of ridged plains and other linea. The next period was dominated by the formation of bands, and the most recent geologic period by chaos formation (e.g., Greeley et al. 2000; Sect. 2). While this relative age relation holds in even the highest-resolution images of Europa thus far obtained (Leonard et al. 2018a,b), Europa Clipper will provide imaging coverage and resolution to confirm these relations, determine detailed deformation history within these broad periods, and understand how it may vary regionally. Additionally, the image coverage to be provided by the Europa Imaging System (EIS) will enable counting of small craters in order to date different terrains, if the signal from secondary craters can be separated out (Bierhaus et al. 2005). Secondary crater rays, which can be tied to the source crater, provide extensive stratigraphic markers for relative ages.

Another way of dating terrains on Europa, at least in theory, may be achieved by the characterization of the radiation-induced modification of surface material. Europa Clipper will observe regions across a range of predicted surface radiation fluxes. The presence and abundance of radiolytically produced compounds detectable by the Mapping Imaging Spectrometer for Europa (MISE) could serve as a metric for total absorbed dose, and thus surface exposure time. Fresh surface materials are subjected to radiolysis and thermal desorption that is expected to loft particulates and gases into Europa's exosphere where they can be analyzed in situ by the MAss Spectromeer for Planetary EXploration (MASPEX). Key non-ice compositional markers in the atmosphere may thus be used to identify geologically young environments relative to older, more radiolyzed surfaces (Teolis et al. 2017; Sect. 3.3).

2.1.3 Global Landform Distribution

Global geologic mapping using Voyager and Galileo data suggests that the locations of landforms may possibly have a longitudinal dependence (Doggett et al. 2009; Leonard et al. 2020). That is, ridged plains appear to be generally widespread over the surface, while bands, cycloids, and other linear features (Sects. 2.2.1 and 2.2.2) appear to be more common in the trailing anti-Jovian quadrant and leading sub-Jovian quadrant (Fig. 1). In addition, chaos terrain appears to be more common in the trailing sub-Jovian quadrant and leading anti-Jovian quadrant (Fig. 1). This apparent longitudinal preference could be related to cross-cutting relations, formation mechanisms, or could be an artifact of the current limited image coverage and the variability in image resolution. EIS is expected to map >80% the globe at scales better than 100 m/pixel, sufficient to resolve these questions.

Additionally, chaos terrain (Sect. 2.2.4) appears to occur more commonly at lower latitudes (Figueredo and Greeley 2004; Doggett et al. 2009). This apparent trend could possibly be related to the distribution of internal heat sources or ice-shell thickness (Ojakangas and

Stevenson 1986). However, the apparent lack of chaos near the poles may be an imaging bias as the Galileo Solid-State Imager (SSI) images of higher latitudes are of low resolution and of limited coverage. Improved coverage provided by EIS will aid in determining the global distribution of landforms.

The global distribution of microchaos (also known as pits, spots, and domes, or lenticulae; cf. Sect. 2.2.7) is also not currently well constrained due to insufficient image coverage at a uniform high resolution. Regional mapping appears has shown that microchaos is more common in the equatorial regions (Greenberg et al. 2003; Culha and Manga 2016; Noviello et al. 2019). It has been hypothesized that this potential clustering of microchaos could correlate with locations where the ice shell is weaker because it is thinner or warmer. To address this, data from the Europa THermal EMission Imaging System (E-THEMIS) (Christensen et al. 2024) will allow us to search for possible associated thermal anomalies (Sect. 3.3), providing a clear link between the interior and the surface geology.

Understanding the distribution of landforms, especially linear tectonic features, across Europa's surface can aid in constraining global stress patterns and provide insight into the processes involved in the evolution of Europa's ice shell. Stresses related to diurnal tides, nonsynchronous rotation, true polar wander, libration, and obliquity may all result in the generation of distinct stress patterns on Europa's surface. Recent analysis has suggested that stresses resulting from true polar wander (Schenk et al. 2008, 2020) and/or obliquity changes (Rhoden et al. 2021) may be responsible for regional-scale, arcuate depressions, a.k.a. "crop circles" (Schenk et al. 2008, 2020; Sect. 2.2.7). Likewise, libration- and obliquity-induced stresses have been proposed to affect the orientation and shape of Europa's cycloids, providing a better fit to the observations than diurnal stresses alone (e.g., Rhoden et al. 2010). Reconstructions of Europa's surface have indicated that plate tectonic-like activity has rearranged portions of the surface in the past, and that this activity may be driven by convection and influenced by global stress patterns (Collins et al. 2022). Testing the driving mechanisms for tectonism on Europa requires global coverage to reveal large-scale patterns as well as sufficient local detail to resolve the type of strain accommodated by tectonic features.

2.2 Regional-scale landform geology

Based on imaging data from the Galileo mission, Greeley et al. (2000) generated a classification system of landforms on Europa divided into seven broad morphological categories: ridges, bands, impact features, chaos, smooth plains, domes, and pits. We follow this nomenclature in the subsections below, briefly describe each category of landform, and review hypotheses from the literature for their formation. We then discuss how observations from Europa Clipper will aid in distinguishing among existing hypotheses. As a mission of exploration, another likely outcome will be completely new hypotheses for these various landforms and any new ones discovered. Note that the categories of pits, domes, small patches of smooth plains (sometimes called "spots"), and chaos areas less than 15 km in diameter have sometimes been grouped together in previous studies under the category of "lenticulae" or "microchaos." (Fig. 2). In the discussion below, we adhere strictly to morphologic categories and do not use the term lenticulae, though we recognize that the similar shapes, sizes, distributions, and clustering of the features described in Sects. 2.2.4–2.2.7 hints at a possible continuum involving similar formation mechanisms (e.g., Pappalardo et al. 1998a,b; Collins and Nimmo 2009; Noviello et al. 2019; Singer et al. 2021).

Because Europa Clipper is designed to execute multiple flybys of Europa instead of orbiting this moon, it is important that the spacecraft trajectory allows sufficient opportunities to examine every subcategory of landform. Most landforms, such as ridges, dilational bands,
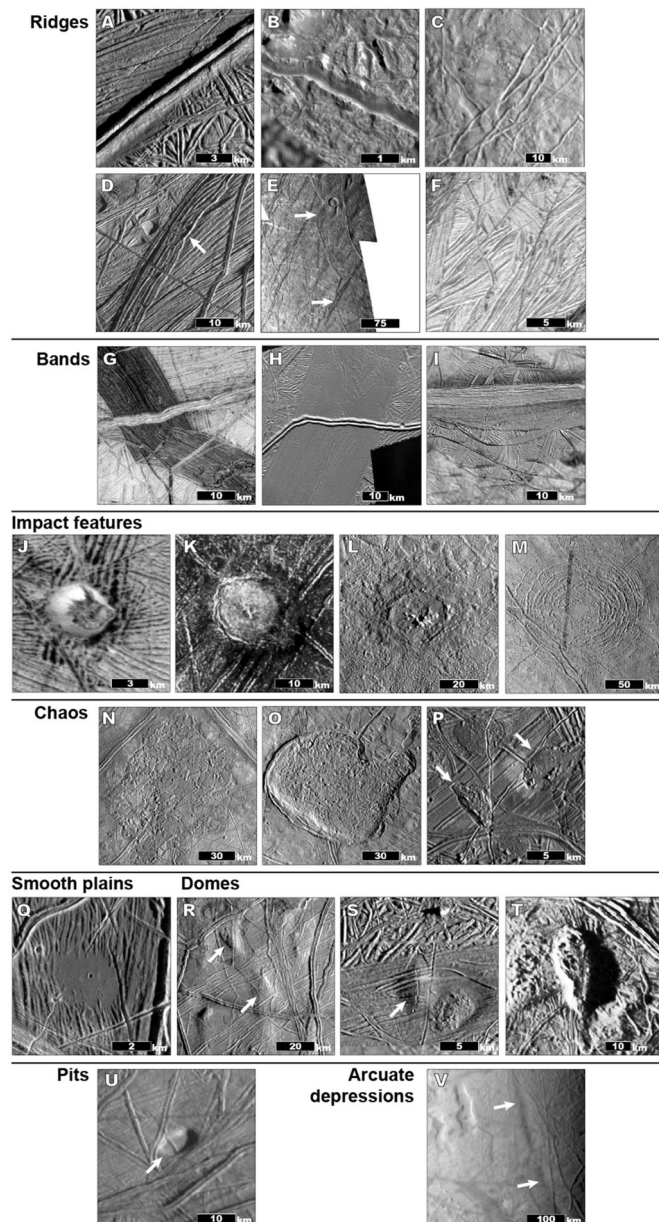
Fig. 2 Examples of landform subtypes discussed in Sect. 2.2. Ridges (Sect. 2.2.1): (A) Double ridge (86°E, 15°N); (B) Trough (86.5°E, 9.5°N); (C) Single ridges (42°E, 2°N); (D) Ridge complex (132°E, 36.5°N); (E) Cycloid (78°W, 56°N); (F) Ridged plains (162°E, 17°S). Bands (Sect. 2.2.2): (G) Lineated dilational band (163°E, 16°S); (H) Smooth dilational band (160°W, 66°S); (I) Bright band (170°E, 40°S). Impact features (Sect. 2.2.3): (J) Simple crater (21°N, 143°E); (K) Regular complex crater (178°E, 2.5°N); (L) Irregular complex crater (89°E, 26°S); (M) Multi-ring basin (147°W, 33°N). Chaos (Sect. 2.2.4): (N) Platy chaos (87°E, 10°N); (O) Knobby chaos (82°W, 22°N); (P) Microchaos (89°E, 9°N). Smooth plains (Sect. 2.2.5): (Q) Smooth plains (33.3°E, 5.5°N). Domes (Sect. 2.2.6): (R) Unbroken domes (132°E, 2°N); (S) Cracked dome (84°E, 9°N); (T) Steep-sided dome (74°W, 43°N). Pits (Sect. 2.2.7): (U) Pit (132°E, 31°N); (V) Arcuate depression (164°W, 27°S).

small impact features, chaos terrain, smooth plains, domes, and pits, are common enough and widely distributed enough that the spacecraft trajectory will pass over multiple examples. For more rare types of landforms, however, it is important to identify trajectories that provide opportunities to study them. Bright bands and arcuate depressions are spatially extended enough to be relatively easy to target, while opportunities to study multi-ring impact basins and potentially active chaos must be carefully assessed during tour evaluation activities (see Sect. 1).

2.2.1 Ridges

Ridges and areally extensive ridged plains are the most common landforms on Europa (Fig. 2A–F) and are subdivided into double ridges, single ridges, ridge complexes, cycloids, and ridged plains. Though there is much variation in specific expression, ridges are generally topographically elevated, quasi-linear, occurring in parallel sets, and they may also be associated with flanking troughs running parallel to the ridge crests. Different subtypes of ridges can grade into one another along a feature's length, sometimes making them difficult to classify. We also include a description of troughs here, as they may be a precursor to ridges.

Double ridges (Fig. 2A) are composed of a pair of subparallel ridges separated by a distinct medial trough. The most common ridge type on Europa, double ridges are found across the ridged plains that cover most of Europa (Fig. 1), with multiple generations of these features cross-cutting each other. Typically, ∼0.5–2 km wide and ∼100–300 m tall, the outer flanks of the ridges usually slope <20°, though the inner slopes bounding the medial trough can be steeper (e.g., Head et al. 1999; Coulter 2009; Coulter and Kattenhorn 2010). Some double ridges run distances of up to ∼1000 km; some run remarkably straight across the surface, likely on great circles (McEwen 1986); while others curve or are sinuous in planform. Vestiges of the underlying terrain can often be traced up the flanks of some ridges (Sullivan et al. 1998; Head et al. 1999).

Models for double ridge formation typically incorporate a combination of tectonic and volcanic processes, though all models are predicated on a pre-existing fracture in Europa's ice shell (Kattenhorn and Hurford 2009). Tectonic models include volumetric deformation under compression (Sullivan et al. 1998; Aydin 2006; Fig. 3A), wedging due to repeated compression (Turtle et al. 1998), uplift of buoyant ice warmed by tidal shear heating along an underlying fracture (Gaidos and Nimmo 2000; Nimmo and Gaidos 2002; Han and Showman 2008; Fig. 3B) or linear diapirism (Head et al. 1999; Fig. 3C). Purely volcanic models include fissure eruptions (Kadel et al. 1998), which may include the simultaneous injection of a liquid sill (Dombard et al. 2013; Craft et al. 2016; Fig. 3D). Johnston and Montési (2014) proposed a case where the freezing of a subsurface liquid water lens deforms the surface, forming single or double ridges, while Culberg et al. (2022) use an analogous process observed in the Greenland ice sheet to show how the refreezing lens would force water toward the central crack area to form the characteristic double ridge morphology (Fig. 3E). Hybrid tectonic-volcanic models typically leverage cyclic tidal forcing on the pre-existing fracture in which ice is added during the opening phase of the tidal cycle, then during the closing phase, that ice is either squeezed onto the surface (Pappalardo and Coon 1996; Greenberg et al. 1998; Tufts et al. 2000; Fig. 3F) or remains in the subsurface to deform the surrounding ice (Melosh and Turtle 2004; Han and Melosh 2010; Fig. 3G).

Single ridges (Fig. 2C) consist of one high-albedo, topographically elevated landform, rounded in cross-section, with a lack of central topographic low or trough. It is unclear if single ridges are an artifact of image resolution (Figueredo and Greeley 2004; Leonard et al.

2018a,b), where the trough of a double ridge is not resolved and therefore the landform appears as a single ridge. These features have not been imaged at resolutions better than 100 m/pixel. If they exist on Europa, single ridges may be part of the evolution from troughs to double ridges (Geissler et al. 1998; Greenberg et al. 1998; Head et al. 1999).

Ridge complexes (Fig. 2D) are intricate and varied landforms that consist of a series of anastomosing or tightly packed ridges and troughs. Individual ridges in a complex may vary from linear to curvilinear and bifurcate along their lengths. Ridge complexes vary in size from ∼500 m to >10 km in width, can run up to hundreds of km in length, and vary in ridge flank morphology from relatively steep and straight to gently convex (Kattenhorn and Hurford 2009; Leonard et al. 2018a,b). Additionally, part of a ridge complex can split or join along its length (e.g., Head et al. 1999; Figueredo and Greeley 2000, 2004) to form multiple complexes.

In some cases, there are subsidiary features found to be flanking prominent ridges and ridge complexes, consisting of parallel broad topographic depressions tens of meters deep on either side, often with sets of small parallel troughs. These flanking troughs are typically interpreted to be the result of lithospheric flexure under the ridge load (Hurford et al. 2005; Dombard et al. 2013). Some of the troughs are observed to contain discrete patches of smooth, low albedo deposits distributed along their lengths that appear to drape over the surrounding terrain (cf. Sect. 2.2.5). Ridges flanked by low albedo material are sometimes referred to as "triple bands" due to their appearance at low resolution as a central bright stripe with two darker stripes on either side.

Ridge complexes may form via a continuation of the double ridge forming process (e.g. Head et al. 1999; Manga and Sinton 2004), and in some occurrences double ridges are observed to grade into ridge complexes along their length (Figueredo and Greeley 2000, 2004). However, some morphological differences between double ridges and ridge complexes are difficult to reconcile, and there may be a gradation from symmetrical ridge complexes to dilational bands, implying a similar origin (Patterson et al. 2010).

Cycloids (Fig. 2E) have similar morphologies as the ridges and troughs described above, but are distinguished as chains of arcuate lineaments, with the arcs being generally of similar sizes (∼100 km long) and convex in the same direction, linked together by sharp cusps (Hoppa et al. 1999c) at an average angle of ∼51° (Groenleer and Kattenhorn 2008). The arcuate morphology of cycloids is generally accepted to result from varying diurnal tidal stresses (Hoppa et al. 1999a,b), possibly with some additional non-synchronous rotation stresses (Hoppa et al. 2001a,b; Hurford et al. 2007; Rhoden et al. 2010) and obliquity (Hurford et al. 2009; Sarid et al. 2009).

Ridged plains (Fig. 2F) (also known in the literature as regional plains, background plains, and ridge-and-trough terrain) is generally the stratigraphically oldest unit on Europa, superposed by every other feature (e.g., Greeley et al. 2000). This unit is characterized by a series of small-scale (∼200–500 m in width) high-albedo ridges in multiple orientations, averaging ∼60 m in topographic relief (Leonard et al. 2020). Ridged plains material covers 50–60% of Europa's surface (Doggett et al. 2009).

Troughs (Fig. 2B), also known as "fissures," are linear landforms with relief of a few hundred meters at most (Schenk et al. 2020) that can extend tens to hundreds of km in length, and are typically 50–500 m in width. These should not be confused with the much wider arcuate depressions discussed in Sect. 2.2.7. They appear to have steep, near-vertical sides and v-shaped cross sections (Pappalardo et al. 1998a,b). Troughs are typically identified as among the youngest features on Europa's surface (Figueredo and Greeley 2004; Doggett et al. 2009; Leonard et al. 2018a,b). Examples have been identified of "raised-flank" troughs, or "proto"-ridges, leading to suggestions that troughs are precursors to double ridges (Pappalardo et al. 1998a,b; Head et al. 1999; Kattenhorn 2002).

All ridge types are sufficiently widespread on Europa's surface so as to allow for many opportunities for them to be investigated by a multiple-flyby mission. Europa Clipper will utilize various types of observations of ridges: The Radar for Europa Assessment and Sounding: Ocean to Near-surface (REASON) will detect thermally or chemically induced dielectric changes including potential subsurface liquid water sills, and salts in the ice if such sills are saline (Buffo et al. 2020; Chivers et al. 2021). Imaging by EIS at multiple scales will reveal detailed morphology, topography, and stratigraphic relations of all ridge types and associated structures, such as flanking troughs and smooth plains. These will be used to test the hypothesis that there is a continuum of morphologies and thus a genetic relationship among the different ridge categories. MISE data will be used to investigate whether low-albedo flanking material is the result of eruptions of subsurface material, and how that material may be related to nearby chaos or smooth plains. Associations between ridges and possible active plumes could be established by a combination of magnetosphere and plasma signatures from measured by the Europa Clipper Magnetometer (ECM, Kivelson et al. 2023), the Plasma Instrument for Magnetic Sounding (PIMS, Westlake et al. 2023), and REASON, particle detections from by the SUrface Dust Analyzer (SUDA) and MASPEX, and/or visual detection of any possible plumes or deposits from EIS, MISE, or the Europa Ultraviolet Spectrograph (Europa-UVS). E-THEMIS measurements may identify regions of recent activity, where the surface may be warmer or the particle size is different from a recent plume material, or where dike/sill injection or shear heating has warmed the material immediately surrounding the ridge.

2.2.2 Bands

Bands are tabular features up to hundreds of km in length, are less than 30 km in width, and are observed across most of the surface of Europa (Schenk and McKinnon 1989; Pappalardo and Sullivan 1996; Leonard et al. 2018a,b). While not as common as ridges, bands comprise ∼3.5% of the total surface area of Europa at the global scale (Leonard et al. 2023). The dominant type of band is known as "**pull-apart**" (Schenk and McKinnon 1989; Pappalardo and Sullivan 1996; Sullivan et al. 1998), or **dilational bands** (Tufts et al. 2000) because they are observed to be areas where extension has opened the surface along fractures. Extension allows fresh material to fill a newly created gap, and in most cases pre-existing features along the band margins can be reconstructed by closing the band. Although the formation process is primarily extensional, in some places there is a component of oblique opening (Tufts et al. 2000; Prockter et al. 2002; Kattenhorn 2004). Dilational bands generally fall into two major morphological subtypes, having either **lineated** (Fig. 2G) or **smooth** (Fig. 2H) textures (Greeley et al. 2000, 2004; Prockter et al. 2002). Both types of bands exhibit bilateral symmetry around a central v-shaped trough aligned parallel to the band margins (Sullivan et al. 1998; Prockter et al. 2002). The relative albedo of dilational bands varies distinctly with apparent age, where the youngest bands have the lowest albedo (dark bands), older bands are of mid-albedo (grey bands), and the oldest bands have the same albedo as the background ridged plains (Schenk and McKinnon 1989; Prockter et al. 2002). Some analyses have suggested that bands brighten with age as a result of radiation exposure (Shirley et al. 2011; Prockter et al. 2017).

A far less common category of bands is that of the **bright bands** (Fig. 2I). Bright bands appear much brighter than the surrounding ridged plains at phase angles greater than ∼40°, though they appear darker than their surroundings at low phase angles (Geissler et al. 1998). Only three examples have been confirmed and mapped (Leonard et al. 2018a,b), for example, Agenor Linea, which is ∼1500 km long and ∼10 km wide. Like dilational bands, bright

bands have similar small-scale internal morphologies, but they do not have bilateral symmetry, and it is not possible to reconstruct pre-existing features along the margins by closing the band (Schenk and McKinnon 1989; Prockter et al. 2000; Greenberg 2004; Kattenhorn 2004).

Analysis from global-scale geologic mapping has suggested that bands may preferentially form on the leading sub-Jovian and trailing anti-Jovian quadrants (Doggett et al. 2009; Leonard et al. 2023). However, it is unclear if this geographic distribution is due to their removal by chaos terrain formation, which is primarily concentrated on the leading and trailing hemispheres. There is no apparent latitudinal preference for band formation (Figueredo and Greeley 2004), though current data is geographically limited.

The bilateral symmetry and internal morphology of dilational bands are strikingly similar to those of terrestrial mid-ocean ridges, leading to suggestions that both may form through similar processes: by upwelling of solid-state material along an axis of extension (Sullivan et al. 1998; Fig. 3H), with band interior morphology indicative of opening rate (Prockter et al. 2002). Such rates have been modeled at 0.2–40 mm/year, similar to terrestrial rates. This suggests the active lifetime of dilational bands may be from 0.1–30 Myr (Stempel et al. 2005). Geodynamic numerical models of icy extension have supported the mid-ocean ridge-like spreading analogy. Plastic necking of the icy lithosphere would occur along an axis of extension, where warm ice from below would be advected upward towards the surface (Mitri and Showman 2005; Howell and Pappalardo 2018), resulting in rifting and the creation of band-like smooth hummocks in a weak lithosphere. Smooth bands with widths comparable to the ice shell thickness may advect material frozen from the ice-ocean interface to the surface on timescales of $\sim 10^5$–10^6 years (Howell and Pappalardo 2018). Another hypothesis for band formation involves progressive ratcheting of a crack open to the ocean, allowing liquid water to erupt and freeze on the surface (Tufts et al. 2000; Fig. 3I). However, this model would be implausible if the ice shell is more than 10 km thick, as inferred from crater morphology (see Sect. 2.2.3).

In addition to the extensional pull-apart bands described above, bright bands (Fig. 2I) may accommodate contractional strain. In fact, bright bands have been shown to have undergone multiple episodes of dilational, contractional, and lateral deformation (Schenk and McKinnon 1989; Greenberg 2004; Kattenhorn 2004; Hoyer et al. 2014; Fig. 3J).

A feature identified as a "subsumption band" as part of a tectonic reconstruction by Kattenhorn and Prockter (2014) is an example of an asymmetric bright band. These investigators theorized that subsumption occurs where one icy slab of lithosphere is forced downward into the ice shell by convergent tectonics before being thermally equilibrated and "subsumed" into the icy interior (Fig. 3K). Whether by subsumption (Kattenhorn and Prockter 2014) or folding (Prockter and Pappalardo 2000; Bland and McKinnon 2012, 2013), there may be a broader class of features that accommodate the contractional strain that would be necessary to balance the extension of dilational bands.

Comparison of detailed morphology, topography, subsurface structure, composition, and any potential thermal anomalies will help elucidate the different mechanisms by which dilational and bright bands are formed. Mapping of Europa's surface at regional scales by EIS will allow a global inventory of band types to be made, reveal their geographic distribution, and allow an assessment of relative ages. These data will also provide essential coverage to allow regional tectonic reconstructions to quantify strain along bands. High-resolution and stereo EIS data will provide detailed morphological and topographic information to assess geodynamic models. For mid-ocean ridge analyses on Earth, imaging data with spatial resolutions of better than 100 m/pixel and topographic data with vertical resolutions of better than 10 m have been used to link surface morphologies to the deep tectonic and volcanic

processes, differentiating between regimes that control surface texture through geomechanical analysis (e.g., Escartín et al. 1999; Buck et al. 2005) and serving as inputs to geodynamic models (e.g., Howell et al. 2016, 2019). Subsurface sounding from REASON will provide information about differences in ice shell structure, composition, temperature, or ice phase beneath bands, as predicted by rifting models, including any evidence of downgoing cold slabs beneath candidate subsumption zones. Composition measurements from MISE as well as in situ measurements from SUDA and MASPEX, would aid in testing the hypothesis that that band material is sourced from the ice-ocean boundary. Compositional data will also help to determine the relative ages and space-weathering states of bands. Currently and recently active extension associated with band formation may be associated with thermal anomalies that could be detected by E-THEMIS. Dilational bands are sufficiently common for there to be ample opportunities for Europa Clipper to observe them. Because bright bands are relatively rare, it will be important to observe at least one of them with multiple instruments, thus they are included in the high-priority Category A landforms in the Geology Planning Guideline (Fig. 1).

2.2.3 Impact features

Impact craters provide insight into surface exposure ages, impactor populations and dynamics, surface properties, and subsurface structure. The latter is of special interest on a body with a subsurface ocean. Europa has one of the least-densely cratered surfaces in the solar system, with few craters ≥30 km (Bierhaus et al. 2009), suggesting an active surface that has erased the earliest geologic history of this icy world. The crater retention age of the surface has been estimated to be between 40 and 90 Myr (Bierhaus et al. 2009; Section 2.1.2). Other evidence supporting a young age includes the observations that very few craters on Europa exhibit tectonic or other geological modification, and a lack of evidence for viscous relaxation (Schenk and Turtle 2009).

Previously, information about small craters on Europa has been limited. The Europan crater population less than 1 km in diameter is dominated by secondary craters and possibly sesquinaries, which are craters formed from impact spall ejected from other Galilean satellites (Zahnle et al. 2008), making it difficult to assess the size-frequency distribution (SFD) of the small primary population. At the scale of tens of meters, Europa's surface is dominated by small pits that appear to be formed from secondaries (Bierhaus et al. 2001, 2005, 2009; Bierhaus and Schenk 2010). The ejecta of young craters contains bright material that has been less altered by the Jovian environment, but extensive visible crater rays are rare on Europa, indicating that rays fade quickly to match the surroundings (Moore et al. 2001; Bierhaus et al. 2009). Some craters exhibit proximal dark or reddish ejecta, suggesting material excavated from certain depths may have a different composition (e.g., Moore et al. 2001; Schenk and Turtle 2009).

From small to large, the craters on Europa can be described in relation to the typical crater morphological categories, with some differences:

Simple craters on Europa are similar to simple craters found on most other icy satellites: bowl-shaped, with a well-defined rim. They have diameters less than ∼4 km, and exhibit a mean depth-to-diameter ratio of ∼0.17 (Schenk et al. 2004). This is smaller than the ∼0.2 value observed on other icy satellites and rocky bodies (e.g., Pike 1980; Robbins et al. 2017 and references therein), though the difference may be due to measurement uncertainty (Bierhaus and Schenk 2010). An example of this type of crater is Niamh (Fig. 2J).

Regular complex craters occur at diameters of 4 to 20 km, and commonly have well-defined rims and flat floors (Moore et al. 2001; Schenk and Turtle 2009) and are morphologically similar to counterparts on Ganymede and Callisto (Schenk et al. 2021). Many of these

craters exhibit small central peaks or peak complexes. In addition, hummocky deposits may be present on the crater floor. Examples of this type of crater include Cilix (19 km diameter) and Rhiannon (16 km diameter; Fig. 2K).

Irregular complex craters are found generally in the 20 to 30 km diameter range. Only four craters in this category have been identified (Schenk 2002; Schenk and Turtle 2009). They have degraded rims, are shallower than expected from smaller regular complex craters and may exhibit lobate flows, proximal dark ejecta, and/or distal bright rays. The interiors can have an anomalous chaotic appearance, including irregular central peak structures and pits. Examples of irregular complex craters include Pwyll (27 km diameter; Fig. 2L) and Mannanán (23 km diameter) (Moore et al. 1998; Moore et al. 2001).

Multi-ring basins appear as an abrupt morphological transition at diameters above 30 km, and are similar to much larger multi-ring basins observed on Ganymede and Callisto (e.g., Valhalla). These structures have no observable rim, are composed of circular hummocky plains surrounded by concentric ridges and graben-like structures, and exhibit low relief (vertical relief of <100 m (Moore et al. 1998; Schenk 2002)). Examples include Callanish (33 km equivalent diameter) and Tyre (38 km equivalent diameter, Fig. 2M).

The morphologies of Europa's impact craters reveal insights into the subsurface structure, in particular the ice shell thickness (e.g., Schenk and Turtle 2009 and references therein). The morphology of the larger impact features on Europa can be attributed to the presence of a subsurface ocean (e.g., Moore et al. 1998), while crater depth/diameter measurements have indicated that the ice shell is ∼10–19 km thick (Schenk 2002; Schenk and Turtle 2009). Some larger impacts may have even penetrated through the ice shell to the ocean (e.g., Greenberg et al. 1999; Cox and Bauer 2015). Irregular complex craters sit at the transition between the expected crater morphology seen on other icy bodies, and the ocean-influenced morphology implied by multi-ring basins. Hypotheses to explain the unusual morphology of these craters include enhanced post-excavation collapse of warm, partially molten subsurface ice (Fig. 3L; Turtle and Pierazzo 2001; Schenk 2002), which could also be modified by brine migration after the impact (Fig. 3M; Steinbrügge et al. 2020a,b), and transient cavities that almost reach the ocean (Fig. 3N; Turtle and Pierazzo 2001).

Data returned by Europa Clipper will enhance our understanding of Europa's craters both individually and statistically. Global imaging by EIS will enable the near-complete characterization of the population of impact craters larger than 1 km in diameter. These data will allow for age determinations of various large-scale units, and will test for leading/trailing cratering asymmetries and longitudinal concentrations of craters, distinguishing planetocentric from cometary impactors. Regional imaging at 25-m pixel scale will enable a detailed view of crater morphology, impact melt, crater rays, secondary fields, and ejecta. Crater degradation states will also be studied using high-resolution images, to investigate resurfacing rates and test the possibility of small- or regional-scale resurfacing events. High-resolution imaging will also enable stratigraphic assessment using superposed features and post-impact modification. Detailed mapping of secondary fields will also clarify the primary SFD at small diameters, as well as providing opportunities for relative age dating from crossing rays.

Stereo data from EIS will be used to create Digital Elevation Models (DEMs), which can be controlled to altimetric measurements from REASON. In combination with Gravity and Radio Science (G/RS), this will reveal depth-diameter relations and morphologic, density, and dielectric variations important to understanding the structure of the ice shell and possible spatial and temporal variations in ice shell thickness. For example, features of multiring basins such as the presence of ring faults, secondary densities (Moore et al. 1998), widths of ring graben (Lichtenberg et al. 2006; Singer et al. 2013) and lack of radial faulting (Turtle

1998; Kadel et al. 2000) have been used to constrain the ice shell thickness, which is one of the primary objectives of the Europa Clipper mission. Better knowledge of crater morphologies will improve these calculations and give ice shell thickness estimates for multiple locations and times in Europa's history. Thus, observations of the multi-ring basins Tyre and Callanish are of high scientific importance to the GWG.

Color, albedo, and compositional measurements by EIS, MISE, E-THEMIS, SUDA, and Europa-UVS will be used to assess differences due to space weathering and heterogeneous subsurface composition revealed in ejecta or central peak structures, or exposed in crater interiors. These instruments may even be able to identify craters with little to no topographic or albedo expression from their distinct compositional or thermal signatures. All of these observation sets together will inform our understanding of the properties of the surface and subsurface, the impacting population, the crater SFD, and ultimately the crater retention age of different areas and features on Europa.

2.2.4 Chaos terrain

Chaos terrain is defined as regions in which pre-existing surface materials have been fractured into irregular blocks or plates which are embedded within a finer-textured matrix material (Carr et al. 1998; Greeley et al. 1998). The possibly related features called "pits, spots, and domes," are discussed separately in Sects. 2.2.6 and 2.2.7. Making up 20–40% of the surface (e.g. Figueredo and Greeley 2004; Neish et al. 2012), chaos is generally considered to be one of the youngest geologic units on Europa (Figueredo and Greeley 2004; Prockter et al. 1999; Doggett et al. 2009; Leonard et al. 2018a,b). In terms of its distribution, chaos appears to be clustered around the equator and on the trailing hemisphere (Pappalardo et al. 1998a; Figueredo and Greeley 2004; Doggett et al. 2009). However, the current lack of uniformity in image resolution may call this conclusion into question.

Recent analyses have suggested that there may be a continuum of chaos morphologies according to the relative ratio of blocks to matrix material (e.g., Collins et al. 2000; Greeley et al. 2000; Leonard et al. 2023). At one end of the continuum, **platy chaos** (Fig. 2N) are relatively large features (e.g., Conamara Chaos, which is >100 km in diameter), consisting of flat or tilted crustal plates or blocks ranging from a few km to tens of km across surrounded by a matrix. The plates may stand up to a few hundred meters above the surrounding matrix (e.g. Carr et al. 1998; Williams and Greeley 1998; Skjetne et al. 2021), and may be translated and rotated from their original positions by up to 5 km (Spaun et al. 1998). Between the plates, the matrix material is lumpy and irregular, and may be found in domes rising several hundred meters above the surrounding terrain (Figueredo et al. 2002; Schenk and Pappalardo 2004). Platy chaos regions are commonly bounded by inward facing scarps, and they may be surrounded by circumferential fractures (Williams and Greeley 1998; Figueredo et al. 2002; Schmidt et al. 2011). On the opposite end of the morphology spectrum, **knobby chaos** (Fig. 2O) (Greeley et al. 2000), is dominated by matrix material, but some preexisting structural features can still be traced through the interior (e.g., Murias Chaos; Figueredo et al. 2002). Knobby chaos may be associated with smooth plains embayment at feature margins, such as at Thrace Macula (see Sect. 2.2.5). Small-scale chaos areas (∼5–15 km diameter) may also be referred to as **microchaos** (Fig. 2P), and these features exhibit the majority of morphological features found in larger chaos regions (Pappalardo et al. 1998a). It has been suggested that large chaos areas may grow from the merging of multiple smaller microchaos (Spaun et al. 1999; Figueredo and Greeley 2004). **Extrusive domes** (also known as Type-1 domes) appear morphologically to be a subset of knobby chaos observed at the microchaos scale, with pronounced updomed topography. Low-albedo

moats of smooth plains (Sect. 2.2.5) have been observed surrounding these domes (Fagents 2003; Nuñez et al. 2019; Quick et al. 2021).

Eight models for chaos formation have been proposed: (1) solid-state diapirism within a thick ice shell driven by thermally (Pappalardo et al. 1998a; Rathbun et al. 1998; Showman and Han 2005) or compositionally (Pappalardo and Barr 2004) buoyant plumes of ice breaking up the brittle surface (Fig. 3O); (2) warm plumes of ocean water melting through the ice shell and causing it to behave as drifting sea ice (Carr et al. 1998; Greenberg et al. 1999; O'Brien 2002; Fig. 3P; see also Goodman et al. 2004); (3) surface breakup due to mobilization of brines trapped within the ice shell (Head and Pappalardo 1999; Collins et al. 2000; Collins and Nimmo 2009; Fig. 3Q); (4) melt lens collapse and freeze-out (Schmidt et al. 2011; Fig. 3Q); (5) injection of ocean water into sills within the ice shell, which then freeze and expand (Collins et al. 2000; Michaut and Manga 2014; Manga and Michaut 2017; Fig. 3R); (6) impact breaching of very thin ice (Cox et al. 2008; Cox and Bauer 2015; Fig. 3P); (7) catastrophic collapse of subsurface void space during heating (Howell et al. 2021; Fig. 3S); and (8) eruption and subsequent extrusion of viscous cryolava flows sourced from gradually freezing fluid reservoirs in Europa's crust (Fagents 2003; Quick et al. 2017, 2021; Fig. 3T). None of these models have satisfactorily explained the observations of all chaos types, including chaos size and the mobility of plates (Collins and Nimmo 2009), and some models may be a better fit for certain types of chaos than others, e.g., the cryolava extrusion models could be a good explanation for knobby microchaos.

The range of proposed models for chaos formation suggest key measurements that can be made to help distinguish which models are viable. Measurements from the Europa Clipper investigations will help to test chaos formation hypotheses by constraining the chemical compositions, the presence of subsurface liquids or salts, relative age relations, and geomorphology among chaos terrains. Topography derived from EIS high-resolution images will allow for detailed characterization of chaos morphology to discriminate between formation mechanisms and allow for potential change detection when compared to Galileo images. Local imaging by EIS at ∼10 s m/pixel will enable characterization of chaos terrain margins and matrix material, including differences between disrupted and fractured ice indicative of dynamic or energetic events (e.g., Collins and Nimmo 2009; Schmidt et al. 2011). The global EIS image dataset at 100 m/pixel will establish a detailed global and local stratigraphy, and identify the distribution of different chaos types. E-THEMIS data may identify thermal anomalies associated with recent chaos formation, as well as the thermal inertia differences between the matrix and block materials; these data will inform formation mechanisms.

The role of liquid water in chaos formation is critical to hypothesis tests (Schmidt et al. 2011). Sounding of the upper ice shell (∼3 km) by REASON will be sensitive to changes in dielectric properties, induced thermally or chemically that may be indicative of distributed past or present subsurface water or salts. Strong reflections from horizontal interfaces may represent the top of extant subsurface liquid water bodies (e.g., Blankenship et al. 2009). Topographic information derived from REASON and EIS data can be correlated with subsurface reflection horizons to determine if the ice is floating in liquid water, as is done for ice shelves and subglacial lakes on Earth (Kapitsa et al. 1996; Corr et al. 2001; Carter et al. 2007). REASON data may also discriminate between surface and subsurface textures and dielectric mixtures that might be consistent with distributed (i.e., "pore filling") water within the ice (e.g., Grima et al. 2017). Any differential penetration between the High Frequency (HF) and Very High Frequency (VHF) bands could help constrain the porosity of matrix materials at depth due to scattering (Aglyamov et al. 2017) and may be able to directly test the catastrophic void collapse hypothesis. Similarly, REASON may detect the presence of subsurface horizons consistent with chaos features that are not expressed at the surface.

Many of the formation hypotheses for chaos vary in the role of near-surface brines, and MISE spectra, plus EIS color images, will confirm the presence and locations of surface salts and variations within different chaos types. The type and concentration of surface salts will provide context for testing chaos formation hypotheses; e.g., extrusive domes may have compositions distinct from the surrounding ice, with different types of extrusive material dependent on compositional evolution of the reservoir through salt concentration and fractionation during freeze out (Chivers et al. 2021; Quick et al. 2019, 2021). SUDA has the ability to characterize salt compositions in situ by analyzing the positive ions and further constrain the negative ions such as chlorides or sulphates in the salts. SUDA measurements will also provide context for the source of materials in chaos areas by detecting organic molecules, water, and other non-water (ice) components in grain particles ejected from the surface (Kempf et al. 2024). As MASPEX will measure gas molecular species that are sputtered from the chaos regions, in particular non-ice compositions, such as organic molecules (Waite Jr et al. 2024). These measurements can help characterize the composition of the chaos terrains and the potential degree of communication with the subsurface in these regions (Teolis et al. 2017).

2.2.5 Smooth plains

Smooth plains (Fig. 2Q) have no visible topographic relief at the limits of Galileo image resolution. They are distinguished as relatively low-albedo contiguous units that tend to fill in topographic lows, embaying and overprinting pre-existing features (e.g., Greeley et al. 1998; Greeley et al. 2000). Smaller plains regions (e.g. Fig. 2Q) commonly occur as discrete subcircular features ~7–15 km in diameter, and spaced ~5–20 km apart. The majority have been identified as "spots" (Pappalardo et al. 1998a,b), and are commonly found in association with other features of similar size (e.g., microchaos, domes, pits), or interspersed with more disrupted chaotic terrain (Pappalardo et al. 1998a,b; Spaun et al. 1998; Prockter et al. 1999; Greeley et al. 2000; Doggett et al. 2009; Leonard et al. 2018a,b, see Sect. 2.2.4). Larger regions of low-albedo plains are found at Castalia Macula (Prockter and Schenk 2005) and around the margins of Thrace and Thera Maculae (Prockter and Schenk 2016), associated with major chaos terrains. The subcircular Castalia Macula plains unit, the largest of its type observed on Europa, is ~30 km in diameter and is estimated to have filled a depression ~350 m deep (Prockter and Schenk 2005). Diffuse, low-albedo, smooth plains material is also found along the margins of large double ridges, extending 8–12 km from the central ridge ("triple bands" (Sect. 2.2.1); Geissler et al. 1998) or as discrete subcircular low-albedo patches spaced along the feature (Greeley et al. 1997; Greeley et al. 1998; Greeley et al. 2000). The plains contain a reddish-brown, non-ice contaminant (Geissler et al. 1998), and are among the darkest features yet found on the Galilean satellites (Helfenstein et al. 1998). Their low albedo and superposition relations indicate that smooth plains are among the youngest features on Europa (e.g., Pappalardo et al. 1998a,b; Doggett et al. 2009; Prockter and Schenk 2005; Leonard et al. 2018a,b).

Several models have been proposed for the formation of low-albedo smooth plains, all of which are related to thermal disruption of ice. Diapiric upwellings or other heat sources within the ice shell could bring the local lithosphere to sufficient temperatures for brine mobilization and migration to occur, leading to ponding of low-albedo, low-viscosity, brine-rich material on the surface (Pappalardo et al. 1998a,b; Head and Pappalardo 1999; Fig. 3U). This model is consistent with smooth plains being associated with chaos terrain, but does not satisfactorily explain the deposits associated with ridges. An associated model suggested that heating of near-surface ice promotes enhanced sublimation of the surface ice,

producing a dark lag deposit of non-ice material (Fagents et al. 2000; Fig. 3V). While this model satisfactorily explains the dimensions of some features, it does not readily explain the smooth, apparently equipotential surfaces of some of the low-albedo deposits. The diffuse dark margins alongside large ridges have been suggested to result from explosive venting of a gas-particle spray derived from a subsurface body of volatile-bearing water (Fagents et al. 2000; Fagents 2003; Fig. 3W), a model that satisfactorily explains the morphology of discrete patches of material, but does not as easily explain the uniformity of contiguous low-albedo smooth plains along other ridges. Dark material found in annular depressions around domes (Sect. 2.2.6) could represent low-viscosity fluids that erupted concurrently with high-viscosity fluids that formed the dome (Quick et al. 2017). In this case, the two fluids would have different compositions. It is possible, if not likely, that the low-albedo plains units on Europa have more than one origin, and consequently may have different compositions.

Measurements from Europa Clipper provide the means to obtain greater insight into the origin of the low-albedo plains material. Local-scale panchromatic and stereo imaging from the EIS cameras will reveal detailed surface texture and morphology, to clearly delineate embayment and other cross-cutting relations. If the plains are cryovolcanic in origin, these data may enable the locations of source vents to be identified. They should also reveal any potential flow features that could identify the direction of emplacement and estimates of material viscosity to be made. If the smooth plains result from explosive eruptions, the EIS data will enable the identification of any blanketing of material around the source region, along with the gradual thinning of deposit margins away from the source. EIS-derived topographic information controlled to REASON altimetry will make it possible to determine whether plains surfaces are equipotential, enabling estimates of eruption viscosity and volume. In addition, color EIS data, near-IR spectral data from MISE, far-UV spectral data from Europa-UVS, and compositional information obtained from SUDA and MASPEX will be used to determine whether the smooth plains material originated from either the ocean or a perched subsurface body of water (see also Becker et al. 2024). Sounding measurements from REASON may be able to constrain the thickness of smooth plains deposits, and could detect thermally or chemically induced dielectric changes indicative of subsurface diapirs or cryovolcanic feeder dikes. Europa-UVS spectral albedo data may reveal variations in the possibly amorphous or (∼50–100 nm) fairy-castle-scale porosity surface structure supporting relative age and possibly source region discrimination. Thermal infrared measurements (regional spatial resolution <250 m) from E-THEMIS will help identify regions of recent activity (via particle size and temperature) and whether smooth plains regolith properties differ from their surroundings, as would be expected in the formation models presented above.

2.2.6 Domes

Domes are positive relief features, typically subcircular to elliptical in planform with diameters between 5–10 km (Pappalardo et al. 1998a,b; Culha and Manga 2016; Noviello et al. 2019; Singer et al. 2021). A few larger domes have been identified, e.g., domes tens of km across are found to the north and south of Castalia Macula (Prockter and Schenk 2005). **Unbroken domes** (also called intrusive domes or uplifts in the literature; Greenberg et al. 2003) (Fig. 2R) preserve the pre-existing structures, landforms and albedo of the terrain they form in, with no apparent fractures or discontinuous features across them (e.g., Carr et al. 1998). **Cracked domes** (Fig. 2S) share many of the same characteristics as unbroken domes, but exhibit one or more fractures on their surfaces, crosscutting the pre-existing material (Carr et al. 1998; Pappalardo and Barr 2004). Unbroken and cracked domes are typically ∼100 m

in relief, with larger domes generally exhibiting larger relief (Singer et al. 2021). These two types of domes do not show any preferred elongation direction, and are most numerous in the trailing anti-Jovian quadrant, tending to cluster near the equator (Culha and Manga 2016; Noviello et al. 2019).

A third type of dome is referred to as **steep-sided domes** (also known as uplifts or massifs) as they are high standing with flat tops and have flanking slopes near the angle of repose (Fig. 2T). The tops of steep-sided domes preserve pre-existing terrain features, and can reach up to 1 km in elevation above the surrounding terrain, making them some of the highest relief features on Europa (Prockter and Schenk 2005). At least 15 such domes have been identified in the global mapping (Schenk 2010; Schenk et al. 2020) and although uplift suggests compressive stresses, their origin remain unknown. Another type of dome, **extrusive domes**, are described in the chaos section above (2.2.4).

Models of dome formation are similar to some proposed chaos formation models (Sect. 2.2.4). Diapir models have suggested that the brittle ice is uplifted from the upwelling of buoyantly rising ice, induced by thermal contrasts and possibly enhanced by compositional segregation (Pappalardo et al. 1998a,b; Rathbun et al. 1998; Sotin et al. 2002; Pappalardo and Barr 2004; Fig. 3X), first forming unbroken domes and then fracturing to create cracked domes from surface curvature induced stresses. Sill injection models suggest that domes are formed by the upwarping of the upper $\sim$1 km of ice from liquid volume added to the ice shell (Michaut and Manga 2014; Manga and Michaut 2017; Fig. 3Y), much like the formation of a laccolith. Freezing of liquid water in a sill would cause volumetric expansion and uplift of the surface (Michaut and Manga 2014; Manga and Michaut 2017; Schmidt et al. 2011; Fig. 3Z).

Global image coverage by EIS along with derived topography derived from EIS and REASON data will provide a means to generate a more complete inventory of dome locations and establish a detailed morphologic classification. In addition, it will be possible to assess any surface changes relative to the data collected by the Galileo spacecraft (e.g., downslope mass wasting or the emplacement of new domes). High resolution morphologic and topographic information could confirm whether dome emplacement is consistent with flexure from intrusive processes (e.g., diapirism, sill injection) along with providing details of these processes (e.g. relative dome height). Specifically, the $\sim$10% difference between the density of water and ice suggests that freezing of subsurface water could create a concomitant positive topographic expression, although this depends on the initial volume distribution of the water (e.g., Michaut and Manga 2014). Unbroken domes likely share a similar surface composition with the surrounding ice, but cracked domes, resulting from upwelling ice diapirs, may expose a contrasting subsurface composition. This may be discernible in high resolution MISE spectral data or in EIS color images ($\sim$tens of m/pixel). Thermal anomalies and differences in thermal inertia across the global population of domes detectable in E-THEMIS measurements may indicate relative emplacement age, and may help discriminate between formation through liquid water or solid-state diapir processes. If a dome is underlain by liquid water, REASON sounding observations could detect radar reflections from the ice-brine interfaces in the shallow subsurface (Blankenship et al. 2009; Culha et al. 2020). As with chaos, the freezing of liquid water bodies, either initially formed by injection or melting in situ, will likely leave behind regions of salt-rich ice or layers of solid salt precipitates (Buffo et al. 2020; Chivers et al. 2021) that would likely attenuate the radar signal or cause a radar reflection, respectively. If compositional or thermal diapirism drives dome formation, REASON data may discern the resulting dielectric contrasts between warm, pure-ice diapirs and the surrounding ice. The detection of sputtered non-salt, outgassed molecules by MASPEX may help to constrain the liquid water composition present under cracked domes (Teolis et al. 2017).

2.2.7 Pits and arcuate depressions

This section will discuss two types of depressions: pits and arcuate depressions.

Pits (Fig. 2U) are sub-circular to irregularly shaped topographic lows where the pre-existing terrain within has not been disrupted. Pits are typically <10 km across and have estimated depths of 200–300 m (Schenk and McKinnon 2001; Greenberg et al. 2003; Greeley et al. 2000; Singer et al. 2021). Pits are less numerous than occurrences of microchaos, but more numerous than domes and small smooth-plains deposits (Noviello et al. 2019). They may preferentially form in the trailing anti-Jovian and leading sub-Jovian hemispheres (Culha and Manga 2016), although this may be related to an observational bias related to the location of near-terminator imaging by Voyager and Galileo.

Due to their similar sizes and spatial associations with domes (Sect. 2.2.6), it is suspected that pits may share a similar formation mechanism. *In situ* melting could explain pit formation, but models differ on whether the isostatic compensation for the volume change is due to melting of warm ocean plumes through the ice shell (Greenberg et al. 1999), or large eutectic melt lenses within the ice shell (Schmidt et al. 2011). Sill injection, as suggested for dome formation (Sect. 2.2.6), could form a pit instead of a dome if the liquid is injected deep enough for the newly added mass to be supported elastically by the brittle ice at the top of the shell (Michaut and Manga 2014; Manga and Michaut 2017; Fig. 3AA). Sills may also be the source of dikes propagating towards the surface by pressurization during solidification, causing depressions as they approach the surface (Craft et al. 2019). Diapiric upwellings induced by the thermal contrast across the ice shell may theoretically reach a few km below the surface (Pappalardo et al. 1998a,b; Rathbun et al. 1998; Pappalardo and Barr 2004) and could induce partial melting near the surface, producing a pit, especially if the diapir is composed of pure ice and impurities are present in the near-surface ice (Sotin et al. 2002; Pappalardo and Barr 2004; Fig. 3BB).

Global mapping of Europa by EIS will allow the current inventory of pit locations, morphology, relative age, and association with other features to be much more extensive. EIS color images along with MISE near-IR and Europa-UVS far-UV spectra can be used to identify any non-ice materials present at the pit locations. In addition, EIS stereo-derived topography will allow the depths of pits and surface morphology to be compared to model predictions. If a region contains recently active pits, the detection of potential thermal anomalies by E-THEMIS could provide information on the role of near surface water in pit formation. Dielectric contrasts detected by REASON will indicate subsurface changes in properties, composition (e.g., salt precipitates; Buffo et al. 2020) or the presence of liquid water that could attenuate the signal or create radar reflections. Warmer or less saline ice diapirs (e.g., Pappalardo and Barr 2004) may also be constrained this way. Furthermore, it might be possible to identify fracture systems in REASON sounding data. These could be interpreted to indicate the presence of conduits for water or fluid movement towards the surface (Michaelides and Schroeder 2019). Similarly, active pits may be outgassing or subjected to sputtering of the fresh surface materials. In this case, MASPEX measurements might reveal a range of chemical molecules that would aid in constraining subsurface composition (Teolis et al. 2017).

Arcuate depressions, also known as "crop circles", (Fig. 2V) are broad (∼25–50 km wide) arcuate topographic lows that can extend hundreds of km in length (Schenk et al. 2008, 2020). Both pits and depressions appear to crosscut almost all preexisting terrain, and their margins range from relatively steep and scarp-like, to gently sloping, with total relief across the depression of ∼300–500 m (Schenk et al. 2008). The terrain within depressions is usually well-preserved and does not appear to be disrupted. The depressions form two incomplete arcs centered near 10°S, 300°E and 10°N, 120°E (Schenk et al. 2008).

Arcuate depressions may have a different origin than pits due to their vastly different horizontal scales, but no subsurface models of their formation process have yet been proposed. In map view, their vast spatial scale suggests that a global tectonic process influences their formation, and they may be related to true polar wander (Schenk et al. 2008, 2020).

2.3 Local-scale surface and near-surface properties

Surface properties provide essential clues to what processes are currently active or were recently active on Europa. Any surface that is apparently less modified by impact gardening, sputtering, and sublimation is likely to have been recently emplaced. Additionally, knowledge of local-scale surface properties is critical for selection of sites for potential future landed surface operations, both to ensure the recognition of sites of maximum science interest, and to optimize the engineering design for mission success (see Section 5; Phillips et al. 2023).

Here, we define local-scale surface properties as those on the scale of a meter, and the shallow subsurface down to a few (<10) meters (Fig. 4). Unlike larger geologic features discussed previously, there are no existing data sets that directly sample the surface of Europa at these scales. For example, Galileo's highest resolution images of the surface were acquired at an order of magnitude coarser pixel scale than expected from EIS. Europa Clipper's improvements on previous data are described in detail in the relevant instrument papers (see other papers in this issue) and their integrated contributions described in Sect. 4. Identification of patterns, textures, block distributions (EIS), and other characteristics of these materials determined from such attributes as their thermal behavior (E-THEMIS and MISE) or radar response (REASON) will be essential in discriminating among various geological process hypotheses both at the local scale and for much larger landforms upon which the fine-scale features are found (e.g. Fig. 3).

Various processes contribute to the landscape and immediate subsurface at local scales, including tectonism, impact cratering, mass wasting, diurnal thermal cycles, sputtering, sublimation, and volatile segregation (Fig. 4). These processes produce small-scale features that might be expected to be observed, including regolith; loose blocks and clasts; ice blades and cups; local extrusions of liquids; and potentially plume deposits (see review in Moore et al. 2009).

Local slopes influence local-scale geologic processes, including mass wasting. The majority of documented mass wasting features occur on steep slopes (Moore et al. 1999; Sullivan et al. 1999) where detached material accumulates at the lowest slope of the flank, creating tongue-like morphology at the terminus (Parekh et al. 2023). The detached mass further disintegrates producing blocky material (Moore et al. 1999) and fine regolith in the form of debris at a local scale on Europa. Mass wasting also produces albedo brightness by exposing fresh subsurface fresh material. All geologic terrain types including crater materials are pervasively sloping on Europa, with mean slopes of 10°–15° on average (Schenk 2009). Smooth areas with low slopes at scales below a few hundreds of meters are rare, consistent with a lack of ancient, relaxed terrains or heavily eroded terrains. However, the length scales at which mass wasting might occur on Europa is not yet known, and available slope measurements are with few exceptions limited to scales of 40 m or more (Schenk 2009).

Ground-based radar observations indicate that the surface layer is porous and/or highly fractured to a depth of at least a few meters (Ostro and Shoemaker 1990; Black et al. 2001; Moore et al. 2009). Models of radar backscatter observations have indicated that the porosity in the upper meter of Europa's ice shell could range from 33% to 94% (Black et al. 2001; Lee et al. 2005). Visible and UV observations suggest hemisphere-averaged surface porosities of
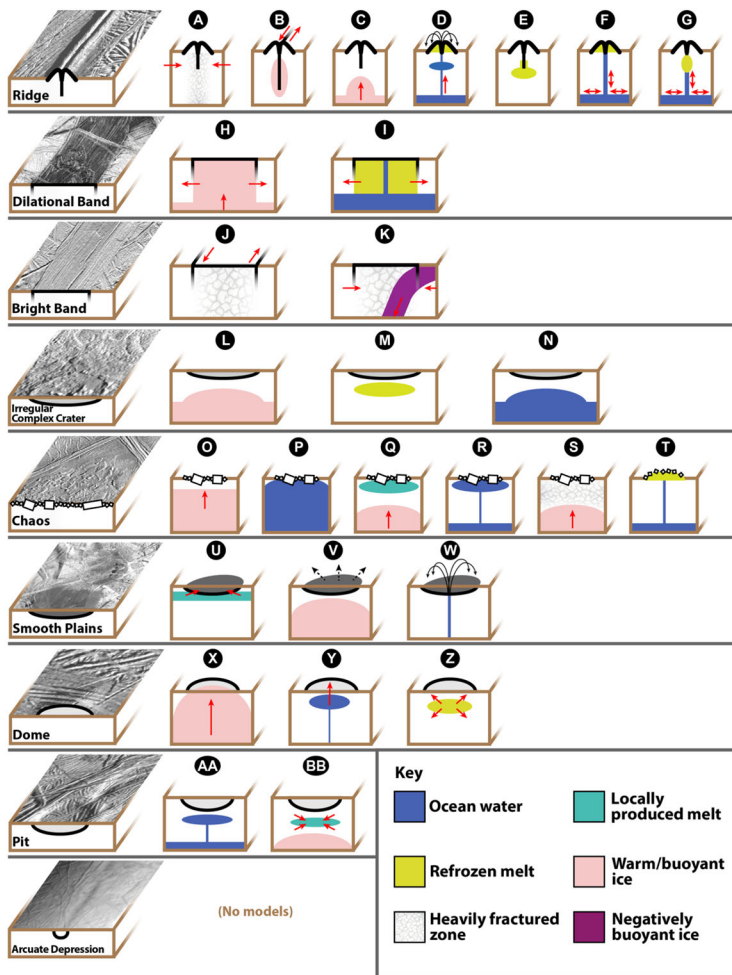
Fig. 3 Theoretical formation mechanisms for Europan landforms. Dark blue indicates the presence of water/brines originating from Europa's ocean, while light blue indicates brines produced within the ice shell. Yellow indicates the importance of refrozen ocean water or local brines in the mechanism. Pink and purple indicate warm/positively buoyant or cold/negatively buoyant ice, respectively. Crosshatch pattern indicates an area of the ice crust intensely processed by tectonic deformation. Red arrows indicate important directions of material motion. Ridge formation hypotheses: (a) compressional crumpling or volumetric deformation, (b) shear heating, (c) linear diapirism, (d) fissure eruption with optional sill, (e) sill freezing, (f) tidal pumping, (g) incremental ice wedging. Dilational band formation hypotheses: (h) mid-ocean ridge like spreading in viscous ice, (i) progressive dilation of a thin separating floating ice crust. Bright band formation hypotheses: (j) combination of strike-slip, extension, and contraction, (k) subsumption or other contractional motion. Irregular complex crater and multiring basin formation hypotheses: (l) collapse over a warm ice substrate, (m) migration and freezing of brine, (n) collapse of thin ice over ocean water. Chaos formation hypotheses: (o) diapirism, (p) disruption of floating thin ice due to melt-through or impact, (q) brine mobilization and migration of trapped melts, (r) shallow sill emplacement, (s) relaxation and collapse of void space over a heat source, (t) extrusion of cryolava. Smooth plains formation hypotheses: (u) expression of mobilized brine onto the surface, (v) enhanced sublimation over a heat source, (w) cryoclastic deposit. Dome formation hypotheses: (x) diapirism, (y) shallow sill injection/laccolith formation, (z) volumetric expansion due to freezing of trapped water body. Pit formation hypotheses: (aa) isostatic adjustment over sill and/or dike emplaced in ice shell, (bb) volumetric contraction due to melting of ice. No local subsurface mechanisms have been proposed to explain the formation of arcuate depressions. Figure by Geoff Collins.

~80–95% for the uppermost micrometers, assuming a uniform grain size distribution, with the sub-Jovian and anti-Jovian hemispheres having higher porosities than either the leading or trailing hemispheres (Domingue and Verbiscer 1997; Hendrix et al. 2005). Although we have a general understanding of the nature of the surface properties, detailed spatial porosity variations and vertical porosity profiles of Europa's near-surface remain poorly constrained. Additionally, models suggest the depth to which millimeter-to-meter scale voids (associated with porosities between 1% and 22%) may extend from hundreds of meters to kilometers (Aglyamov et al. 2017; Nimmo et al. 2003), depending on the balance of processes that either create porosity (e.g., impacts and tectonic fracturing) or those that tend to remove porosity (e.g., sintering). As such, the array of Europa Clipper instruments and their associated data sets will be brought to bear to increase our understanding of the properties of the Europa surface.

Understanding the porosity of the Europan regolith will be important for understanding its origins, composition, and processing. REASON is sensitive primarily to the ratio of void space (porosity) in ice at the surface. Compact ice (no porosity) is approximately 5 dB more reflective than old fallout that has been sintered and plastically deformed (porosity >0.5). Old deposits, in turn, are significantly more reflective than fresh deposits dominated by gravitational rearrangement (porosity >0.9) (Grima et al. 2014b). REASON reflectometry measurements will attempt to disentangle the effects of porosity from those of scattering from a rough surface to better assess variability in ice porosity. At the surface, porosity can be derived through photometric modeling of the solar phase curve reflectances measured by EIS, MISE, and Europa-UVS (e.g., Domingue and Verbiscer 1997; Hendrix et al. 2005). The number of Europa Clipper flybys at a variety of geometries will allow for robust measurements reflectance across different phase angles and in different regions of the surface, which will constrain variations in ice porosity.

Thermophysical properties of Europa's surface will be of particular interest in illuminating the nature of the regolith. Surface temperatures from the Galileo Photopolarimeter-Radiometer (PPR) have been used to determine the thermophysical properties of Europa's surface at higher resolution (Rathbun et al. 2010, 2014; Spencer et al. 1999). Europa's average albedo (0.56) is higher than that of the other Galilean satellites, and its average thermal inertia (69 J m^{-2} $s^{-1/2}$ K^{-1}) is among the highest observed for any icy satellite (Rathbun et al. 2014). Higher thermal inertias are usually indicative of denser surface materials. Due to the PPR's relatively low resolution, these data are only indicative of the bulk properties of the surface at regional scales. Data from the Atacama Large Millimeter Array (ALMA) have also been used to derive a slightly higher global thermal inertia of 95 J m^{-2} $s^{-1/2}$ K^{-1} (Trumbo et al. 2018). Spatial variations in thermal inertia may not be correlated with very large-scale surface geologic units, but they might be reflecting material characteristics at a greater depth.

Telescopic measurements acquired during solar eclipses by Jupiter have also been analyzed to constrain the structure of the upper regolith (Hansen 1973) over a smaller vertical length, but with a higher vertical resolution. The regolith on Europa appears to be strongly layered: the top few millimeters have a low thermal inertia, and underlying that is a much higher thermal inertia layer, consistent with very fine particulate material on top of an indurated/solid ice layer. These results have been interpreted to indicate actively self-healing regolith through an undetermined process (e.g., Molaro et al. 2018).

While individual Europa Clipper instruments will produce informative observations at the local scale, the combination of observations will profoundly constrain local surface properties to a much greater degree. For example, local surface characteristics will be determined from a combination of EIS local scale, panchromatic, and stereo data for an array of geologically diverse sites and at scales down to ~0.5 m, with EIS 10-m-scale data providing
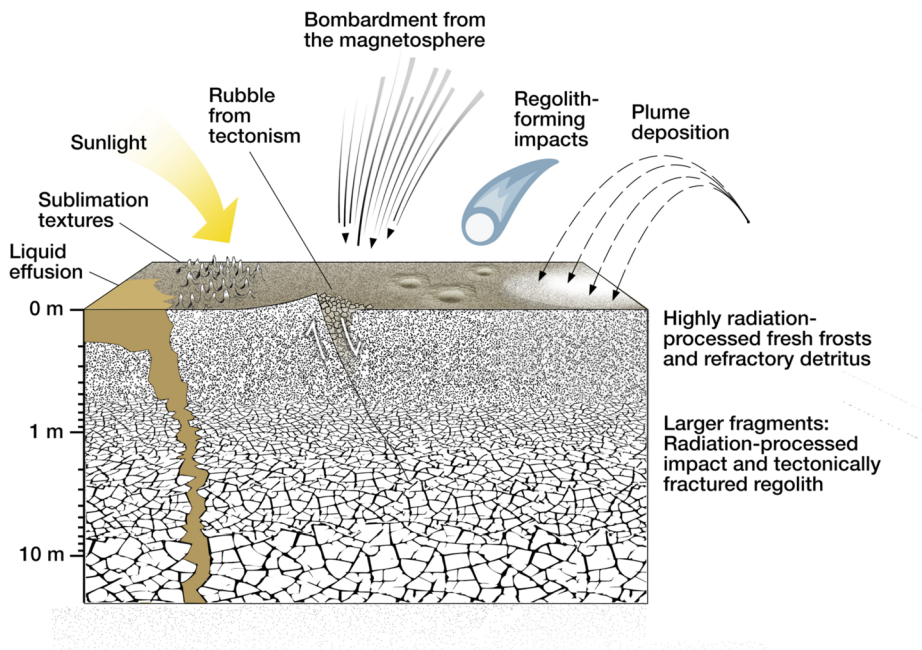
Fig. 4 Schematic visualization of the near surface structure of Europa's ice shell. The vertical scale is logarithmic. This schematic represents a model that is internally consistent with infrared and radar observations. Europa's surface is modified by high-energy sputtering of material and impact gardening, by sublimation due to insolation, condensation, and possibly by cryovolcanic resurfacing processes (possible plume deposits; the eruption onto the surface of water or brine; and surface destabilization by melt-through from beneath). As described in the text, Europa Clipper's suite of instruments will penetrate the near surface to different depths and will reveal surface physical structure, composition, and properties. Figure by David Hinkle.

an intermediate scale link between regional and local scales (see also Sect. 4). These products are directly comparable to the high-spatial resolution multispectral cubes that will be obtained by MISE at dozens of sites at resolutions as good as $\sim$10 m (Blaney et al. 2024). Measurements of diurnal temperature variations by E-THEMIS, when combined with those from MISE (composition) and REASON (near-subsurface structure), will aid in constraining the small-scale physical and thermophysical characteristics of the surface. Such characteristics include grain size, small scale roughness, near-surface temperature as a function of depth, and thermal inertia, which will provide constraints on density and thermal conductivity. MASPEX will make measurements of Europa's tenuous diurnal atmosphere, which cycles through thermal adsorption and desorption processes. E-THEMIS and MASPEX observations combined will facilitate the characterization of exchange processes between thew surface regolith and the atmosphere (Teolis et al. 2017; Waite Jr et al. 2024). Altimetry and reflectometry measurements made by REASON will constrain surface topography, regolith cohesiveness, thickness and subsurface layering, and surface roughness. Furthermore, joint analysis of REASON VHF and HF reflectometry data will help to constrain the average porosity within 150 m of the surface as described above (Chan et al. 2023). Block abundance models can be developed using EIS NAC, E-THEMIS, and REASON observations of the same locations and then extrapolated to regions with more limited data available.
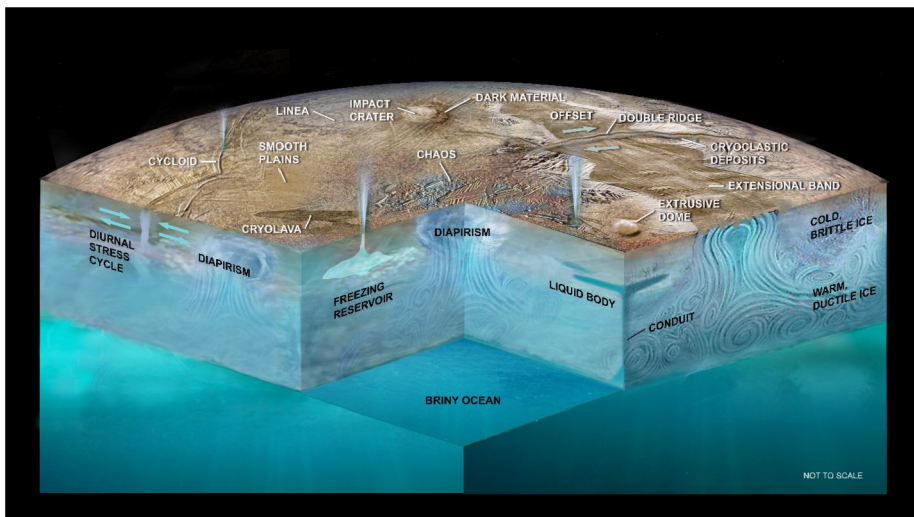
Fig. 5 Schematic of a cross-section through the icy crust of Europa showing hypothesized processes (described in the text) that might generate plumes, cryovolcanic surface features, and other morphology indicative of current activity. The ice shell is shown as a cold, brittle shell over a warmer, more-deformable ductile layer, above a global briny ocean. The ice shell is subject to powerful stresses that can first form and then open and close cracks and conduits, the latter providing indirect pathways for water into the ice shell. These strong tidal stresses contribute to the formation of cycloids, ridges, and extensional bands. The effects of diapirism within the ice shell can penetrate to the surface, leading to melt-through and resurfacing. Diapirism and shell fracturing can lead to the formation of liquid reservoirs within the brittle ice. Stresses in these reservoirs as the water or brine freezes may lead to the opening of conduits to the surface, the generation of plumes, the formation of domes, or the emplacement of "cryolavas" or smooth plains. Figure by David Hinkle.

3 Current activity

The lack of a heavily cratered surface is an indication that Europa is geologically young, (see Sect. 2.2 and associated references), but it is not yet known if the moon is active today. An important aspect of the Europa Clipper mission will be to provide a greater understanding to the degree that this icy world may be currently active (Fig. 5). The moon's extremely young crater retention age (∼40–90 Myr, Sect. 2.2.3) suggests that geologic processes have acted in the recent past to erase older terrains – processes which may continue to the present day and thus could be directly or indirectly observable by Europa Clipper. These processes could include cryovolcanism, tectonism, geyser-like plumes, impact cratering, or any of the formation mechanisms discussed in Sect. 2.2 for recent landforms such as chaos terrain or young ridges/bands (Fig. 4). Evidence of current surface activity (or lack thereof) will shed light on which of these processes may continue to be active today, and thus what the driving forces are for geologic change on Europa. Active processes could indicate whether a subsurface ocean is present today, constrain the thickness of the ice shell, place bounds on the proximity of intra-ice pockets of liquid water to the surface, allow improved constraints to be placed on rates of surface–subsurface exchange, provide a means to estimate the rate of space weathering, and complement other constraints on relative surface ages.

In this section we discuss what is currently known about possible plumes on Europa and how Europa Clipper will search for and characterize them (Sect. 3.1); thermal anomalies that might accompany current geologic activity such as volcanic or tectonic activity (Sect. 3.2); and other indications of current activity such as direct observations of surface activity or

changes since the Galileo mission of the 1990s, and detection of fresh materials (Sect. 3.3). Figure 4 illustrates the various forms these processes could take and their possible surface expressions to be investigated by Europa Clipper.

3.1 Possible Plumes

Cryovolcanic activity in the form of geyser-like plumes and surface flows may play a role in the resurfacing of Europa. Low-albedo deposits surrounding lenticulae and along lineaments on Europa might be cryoclastic mantlings that were ballistically emplaced during cryovolcanic eruptions (Fagents et al. 2000). In addition, features such as lenticulae and chaoses may be the surface manifestations of internal cryomagmatic processes (i.e., diapirism) (e.g., Wilson et al. 1997; Pappalardo et al. 1998a,b, 1999; Prockter and Schenk 2005). Ultimately, as images and NIMS data from the Galileo mission have revealed features indicative of effusive cryovolcanism, including low-albedo plains and extrusive domes (e.g., Fagents 2003; Kattenhorn and Prockter 2014; Prockter et al. 2017; Quick et al. 2017, 2022), cryomagmatic intrusions (e.g., Rathbun et al. 1998; Figueredo et al. 2002; Sotin et al. 2002; Craft et al. 2016; Manga and Michaut 2017; Chivers et al. 2021), and possible cryoclastic deposits (e.g., Fagents et al. 2000; Quick et al. 2013; Quick and Hedman 2020), it is reasonable to hypothesize that venting in the form of geyser-like plumes may also occur as part of a continuum of volcanic processes on Europa.

3.1.1 Mechanisms of plume eruptions

Cryovolcanic eruptions may occur when: (1) cracks induced by rising diapirs expose volatile-rich water to Europa's zero-pressure surface environment (Crawford and Stevenson 1988); (2) the convergence of ascending diapirs with tidally generated cracks in Europa's shell produce dikes capable of transporting volatile-laden water to the surface (Head et al. 1999; Phillips et al. 2000; Fagents 2003); or (3) excess pressures caused by the gradual freezing of crustal fluid reservoirs, or by tidal stresses acting on crustal fluid reservoirs, cause fractures to form in Europa's ice shell that transport cryovolcanic fluids to Europa's surface (Fagents et al. 2000; Fagents 2003). Recent models have suggested that eruptive venting associated with chaos formation or the migration and subsequent crystallization of brine pockets associated with impacts may also trigger plume eruptions on Europa (Walker and Schmidt 2018; Steinbrügge et al. 2020a,b). While the former mechanism could release enough energy to result in sizeable eruptions and plumes up to 150 km tall, the latter would produce plumes of the order of only a few km in height. Indeed, based on the average impact frequency and impactor size at Europa, it is unlikely that impact events would trigger sizable plume eruptions (Roth et al. 2014b). Each of these plume mechanisms would also result in endogenic heating of the surface that would result in a thermal anomaly (see Sect. 3.2). The dissociation of clathrate hydrates in the icy crust (Prieto-Ballesteros et al. 2005; Hand et al. 2006) may also trigger eruptions, similar to what was proposed for Enceladus (Kieffer et al. 2006) and may potentially result in the explosive release of large quantities of volatiles in addition to water vapor.

Existing theoretical models for explosive venting on Europa include ballistic models, which focus mainly on the particle component of Europa's plumes and their associated deposits (Fagents et al. 2000; Quick et al. 2013; Quick and Hedman 2020). These suggest that Europa's potential plumes may be relatively small (<30 km high). These models also predict that plumes most likely leave behind low-albedo deposits along lineaments and perhaps in association with domal lenticulae. In addition to particulates, Direct Simulation Monte

Carlo (DSMC) models have focused on the vapor component of plumes (Berg et al. 2016), while other models have taken an integrated approach, assessing potential effects of Europa's plumes locally and on its global exosphere (Teolis et al. 2017).

3.1.2 Searches for and indications of plumes on Europa

Previous studies have searched for evidence of plume deposits on Europa's surface utilizing several of the same methods that have been employed to observe plumes on other active moons such as Io, Triton, and Enceladus (Pappalardo et al. 1999; Phillips et al. 2000). Low-resolution and low-signal-to-noise Voyager observations of two anomalously bright features on Europa were initially interpreted to be evidence of plume activity, with one feature interpreted to be a plume and the other as the resulting deposit (Cook et al. 1982, 1983; Helfenstein and Cook 1984). However, subsequent analyses did not confirm these observations (Pappalardo et al. 1999), and the anomalous features may have only appeared to be exceptional because, unlike other bright areas on Europa's surface, they were imaged at high phase angles (McEwen 1986). Other searches for active plumes on Europa involved the collection of a single set of Galileo Solid State Imaging (SSI) frames along the bright limb and detailed comparisons of Voyager and Galileo data in an effort to detect surface changes. These investigations yielded no definitive evidence of large-scale venting (Phillips et al. 2000; Schenk et al. 2020), possibly due to Europa's unfavorable stress state and orbital position at the time of observation (Hoppa et al. 1999a,b; Phillips et al. 2000), and suggested that any plume activity that is currently occurring on Europa may be episodic, produce no observable effects, and/or may occur over small areas of the surface. Cursory plume searches comparing images from Galileo and New Horizons yielded no additional evidence of plume activity on Europa (Quick et al. 2010; Bramson et al. 2011; Schenk 2020). This may be in part because image scales less than ∼100 m/pixel may be needed to observe Europa's plumes (Phillips et al. 2000). Searches for endogenic thermal emissions in Galileo observations were also unsuccessful, but the data are limited in extent (Rathbun et al. 2010; see Section 4.3.2).

Observations of Europa by the Hubble Space Telescope (HST) using two different observing techniques have yielded evidence consistent with some characteristics of plumes. Roth et al. (2014a) discovered hydrogen and oxygen line emission beyond the limb of Europa, consistent with the dissociation of a water vapor plume up to 200 km in height located near the south pole. Column densities for these candidate plumes were estimated to be of the order of 10^{16} molecules/cm^2. Such plumes would be vapor dominated and particle poor. While follow-up observations of the same type did not yield similar detections (Roth et al. 2014b), Sparks et al. (2016) found evidence for continuum absorption beyond Europa's limb as it transited Jupiter. Three out of their ten observations were interpreted to be consistent with plume activity, two at latitudes similar to those identified by Roth et al. (2014a). One source location, just north of the Pwyll impact crater, was observed again by Sparks et al. (2017) and is coincident with a thermal anomaly observed by Galileo PPR (Spencer et al. 1999). However, follow-up analysis of the thermal data showed that the anomaly was not endogenic (Rathbun and Spencer 2020). Furthermore, a later detailed analysis of the statistical and systematic uncertainties showed that the features interpreted as plumes in Sparks et al. (2016) were consistent with random statistical occurrences (Giono et al. 2020). One general problem in the search for anomalies in the HST transit images is that the position of Europa on the detector is unknown. Thus, small misalignments of only one pixel can create artifacts. The trailing hemisphere limb, where all suspected plume features reported in Sparks et al. (2016) are located, is particularly sensitive to these effects.

Recent observations with the Keck telescope providing direct detection of water vapor, as opposed to its dissociation products or ultraviolet absorption, suggested that, if present,

Europa's plumes may be somewhat smaller than previously estimated, with vapor column densities of the order of 10^{15} molecules/cm^2 (Paganini et al. 2020). These authors suggested that venting leading to large plumes that are hundreds of kilometers tall may be the exception rather than the rule on Europa, in agreement with previous Galileo image analysis and theoretical modeling suggesting that venting on Europa may be small-scale in nature (Fagents et al. 2000; Phillips et al. 2000; Quick et al. 2013).

Recent re-analyses of particles and fields data acquired by the Galileo spacecraft during its close encounters with Europa have yielded additional evidence that is consistent with the presence of plumes. On the Galileo E12 flyby of Europa, which was that spacecraft's closest encounter with the moon (closest approach altitude $\sim$ 206 km), the spacecraft observed abrupt changes in the magnetic field and localized enhancement of plasma density near the equator on the trailing hemisphere (Jia et al. 2018). By using a multi-fluid magnetohydrodynamic (MHD) simulation, Jia et al. (2018) showed that the observed magnetic field and plasma density variations are consistent with the spacecraft passing through a vapor plume with characteristics similar to those inferred from the HST observations. In addition to the E12 flyby, the only other Galileo flyby that came within 400 km of Europa's surface was the E26 flyby. Based on a hybrid plasma simulation, Arnold et al. (2019) suggested that the magnetic field variations observed near closest approach during the E26 flyby can be explained by the spacecraft passing through a plume near Europa's south pole, although it has more recently been demonstrated that these observations could be explained by instrument artifacts (Jia et al. 2021).

Given their likely sporadic nature, and in the absence of direct detection, their associated deposits could enable constraints on the locations, eruption rates, sizes, and composition of any plumes that may have emplaced them. In addition, owing to their minimum exposure to Europa's severe radiation environment, fresh plume deposits could contain and preserve organic compounds from the interior (e.g., Nordheim et al. 2018). Their potential to contain biomarkers thus makes their identification a critical step in constraining Europa's habitability potential. Recent analyses of Voyager, Galileo, and New Horizons data have revealed no evidence of color or albedo changes representative of surficial plume deposits between 1979 and 2007 (Schenk 2020), but the wealth of new data from the Europa Clipper payload will expand the spatial, temporal, and wavelength range of possible deposit detections.

3.1.3 Europa Clipper plume search and characterization strategy

If detected, plumes on Europa's may not be tidally controlled, may be sporadic in nature (Roth et al. 2014b; Rhoden et al. 2015), and unlike Enceladus' plumes, may not be tied to any specific region on the surface. In addition, their output and intensity may be markedly different from Enceladus' plumes, due to differing gravity, differences in subsurface plumbing systems, and/or differences in the stress states of their ice shells (Hansen et al. 2019). Consequently, Europa Clipper may need to employ indirect means to locate plumes and constrain their eruption frequency. Europa Clipper's integrated plume search strategy includes investigations by EIS, E-THEMIS, MISE, Europa-UVS, REASON, MASPEX, ECM, and PIMS, which are designed to identify plumes and constrain their properties.

As was demonstrated by the Voyager, Galileo, and Cassini imagers at Io (and Enceladus by Cassini), and more recently at Europa with the HST, Space Telescope Imaging Spectrograph (STIS), plume searches and detection can be conducted by direct imaging and monitoring of the limb of a moon (McEwen et al. 1998; Sparks et al. 2016). Thus, EIS will image Europa's disc near the limb at high phase angles and along the terminator in an effort to detect the particle component of any plumes. High phase angles are preferred because small

forward-scattering plume particles would be brightest and the moon's bright limb is darker, thus contributing less stray or scattered light that complicates plume detection. In addition, change detection with the EIS color filters will allow the imagers to search for effusive eruptions, which could be spatially located near areas of eruptive venting and represent evidence of fresh deposits on the surface.

Thermal infrared measurements of Europa, both in and out of Jovian eclipse, could also reveal hotspots and limb features indicative of plumes and recent surface activity (Johnson et al. 1984; Sparks et al. 2019). E-THEMIS and MISE data will also be used to search for endogenic heat sources that could be associated with plumes (see Sect. 3.3). Moreover, E-THEMIS measurements could be used to detect variations in thermal inertia caused by the emplacement of fresh plume deposits on Europa's surface: Plume fallout may reduce thermal inertia if plume particles dominate and are small, or deposition of plume gases may increase thermal inertia due to sintering of surface grains (e.g., Rathbun et al. 2004; Christensen et al. 2024). MISE spectra should also be able to reveal any diffuse patches of differing composition on Europa's surface created by fallen plume material. Europa-UVS scan observations may capture ongoing plume eruptions via hydrogen and oxygen line emission (Roth et al. 2014a), transit imaging (e.g., Roth et al. 2017), and stellar and solar occultations emphasizing the gas component, as well as gathering surface albedo datasets to identify unique compositional and microphysical surface deposits possibly due to recent plume activity. Additionally, the possible bisection of an active plume by one or more of the many planned stellar occultation observations could return detailed composition and vertical structure information of any plumes, well sampled over different timescales throughout the mission. REASON's contribution to the search for and study of Europa's candidate plumes will take two forms. First, relative timing delays between REASON VHF and HF surface echoes will be used to characterize the ionospheric electron density in the vertical column between the Europa Clipper spacecraft and the surface (Grima et al. 2015; Scanlan et al. 2019; Blankenship et al. 2024, this collection) where any local anomalies may be indicative of ongoing plume activity. Second, REASON reflectometry measurements will provide insight into porosity or near-surface layering (see Sect. 2.3) that could be related to plume deposits.

Active plumes can enhance global water signatures and multiple other plume species, including noble gases, nitrile and organic species, significantly altering the global composition of Europa's tenuous atmosphere (Teolis et al. 2017; Lee et al. 2005; Becker et al. 2024). Models suggest that a recent plume could produce signature exosphere compositions (as a ratio to O_2) that would be detectable far from the plume by MASPEX (Teolis et al. 2017). Global enhancements due to active plumes may not be able to localize the source, but would provide compelling evidence of current activity.

If active plumes are located, in situ analyses with MASPEX and SUDA could further provide characterization and compositional analysis of the plume materials. Along the spacecraft trajectory, MASPEX will measure the spatially resolved density and chemistry of the exosphere, which is predicted to differ in terms of structure and composition in the presence of contemporaneous plume activity. SUDA has the capability of determining the mass, size, and composition of non-ice components such as organic molecules as well as salts of the grain particles of possible plumes. Negative ion detection and characterization could provide further constraints on the salinity of the liquid reservoir from which a plume could be sourced. In addition, SUDA measurements can also provide chemical compositional analysis of any recent plume deposits on Europa's surface when flying over those areas at lower altitudes (∼35 km or below).

A plume may generate perturbations to its surrounding magnetic field and plasma environment through interaction with Jupiter's magnetospheric plasma. ECM and PIMS will be

able to detect localized perturbations in the magnetic field and plasma properties, respectively, that may be associated with a plume, such as changes in magnetic field strength and orientation and variations in plasma density and flow velocity.

3.2 Thermal anomalies

The most common endogenic thermal anomalies observed with remote sensing throughout the solar system are the result of volcanism, but they can also be formed by tectonic and other geological surface processes. Most of these processes are associated with movement of material from the subsurface to the surface, which, for Europa, makes any thermal anomaly a high-priority target for probing the interior of Europa, as it may indicate an area where organic material could have been transported from more habitable portions of Europa to the surface.

Plumes on Io and Enceladus are accompanied by thermal anomalies at the surface (Spencer et al. 2006; Davies 2007). Any cryolavas that are warm enough (∼200 K) to flow (e.g., Quick and Marsh 2016) would also be detectable by E-THEMIS as thermal anomalies on Europa's surface (Christensen et al. 2024), which is typically 70–90 K on the nightside and less than 130 K on the dayside (Rathbun et al. 2010). In addition, MISE is capable of detecting such thermal anomalies in both day- and nightside observations if the anomaly is at or greater than ∼190 K and fills more than 10% of a pixel (Blaney et al. 2024).

Besides some limited coverage by the Voyager spacecraft (Spencer 1987), the only spatially resolved datasets of Europa's temperatures are from the Galileo PPR instrument (80–300 km resolution; Spencer et al. 1999; Rathbun et al. 2010) and the earth-based ALMA (∼200 km resolution; Trumbo et al. 2018). Both sets of observations have successfully been modeled as passively reradiated solar radiation and showed no obvious thermal anomalies. Additionally, only a few percent of Europa's surface were covered by the PPR with enough detail to conclude that liquid water did not exist in these regions (Rathbun et al. 2010). Those observations were concentrated near Europa's leading and trailing points, leaving much of Europa's surface unexplored in the infrared wavelength range.

3.2.1 Possible sources of thermal anomalies

Thermal anomalies may result from active resurfacing exposing warmer subsurface material, shallowly buried warm material, or active or recent plume vents or deposits. Several types of geologic features on Europa are young and possibly formed by water or warm ice. In particular, chaos regions may be formed by the extrusion of warm ice onto Europa's surface (see Sect. 2.2.4). Based on the average surface age, Abramov and Spencer (2008) have suggested that the number of detectable thermal anomalies on Europa's surface should currently be 1 to 10 if recent resurfacing is dominated by the formation of chaos regions with areas of 100 to 1000 km^2. Alternative models propose that chaos could form over large lenses of liquid water in the shallow subsurface (Schmidt et al. 2011). It has been hypothesized that such features could be detectable for thousands of years after the activity ceases (Abramov et al. 2013). Regardless of the formation method, a near-surface thermal anomaly associated with a 100-m-thick layer of liquid water may be detectable for at least several hundred years (Abramov and Spencer 2008).

Tectonic deformation may also create thermal anomalies associated with geologic landforms. On Europa, tectonic deformation occurs pervasively through extensional (e.g., Prockter and Patterson 2009) and strike-slip (e.g., Hoppa et al. 1999b) fault activity, with few observations of potential convergent activity (Prockter and Pappalardo 2000; Kattenhorn

and Prockter 2014; Collins et al. 2022). Activity associated with extensional bands probably draws relatively warm and buoyant ice material upward, increasing near-surface heat flow regionally, and may dissipate heat frictionally on normal faults (Fig. 3), potentially producing local thermal anomalies (Howell and Pappalardo 2018). While robust stratigraphic information for Europa is limited, it has been suggested that the onset of band formation in the geologic record pre-dates the onset of chaos formation (Figueredo and Greeley 2004; Doggett et al. 2009). This indicates that extensional tectonics on bands may not be the most recent style of activity, and may not continue to the present day. Strike-slip features may dissipate frictional heat that potentially induces melting, producing anomalies indicative of recent or ongoing activity (Gaidos and Nimmo 2000; Nimmo and Gaidos 2002; Kalousová et al. 2014). In comparison to extensional features, convergent tectonics may depress isotherms regionally, resulting in cold surface anomalies with local warm spots due to friction dissipation on thrust faults (Kattenhorn and Prockter 2014).

3.2.2 Europa Clipper Thermal Anomaly Search Strategy

There are two instruments on Europa Clipper that will contribute to the search for thermal anomalies. E-THEMIS will acquire thermal infrared images of Europa in three spectral bands ranging from 7 to 50 microns (Christensen et al. 2024) while MISE will cover a spectral range of 0.8 to 5 microns (Blaney et al. 2024). E-THEMIS will resolve 50-m surface features to accurately determine surface temperatures $> \sim$60 K, while MISE is sensitive to thermal emission from the warmest possible areas that may be present on Europa. Acquiring measurements of anomalous thermal emissions from both instruments would provide strong constraints on the temperature and area distribution present.

One way to distinguish between temperature anomalies due to different thermophysical surface properties and endogenic heating is to measure temperatures during both the daytime and nighttime (Rathbun et al. 2010). E-THEMIS will obtain day- and nighttime coverage at better than 20 km/pixel resolution element over more than 80% of Europa's surface. This global dataset will be able to detect endogenic thermal anomalies comparable in magnitude to the Enceladus south polar tiger stripes over most of Europa's surface.

Thus, E-THEMIS and MISE datasets, which will both cover most of Europa's surface, will enable unambiguous determinations of which features on Europa are very young and still geologically active. The locations and spatial distribution of such thermal anomalies will place constraints on models of resurfacing mechanisms (e.g., conduit-like or linear vent, surface flows, melt-through area). These models, in turn, inform interpretations of the specular and scattered components of the radar surface echoes acquired by REASON (Grima et al. 2014a,b).

3.3 Surface activity evidence

Evidence of modern geologic activity on Europa is of acute interest because it would indicate the current status of Europa's habitability. Plumes and their deposits (Sect. 3.2), thermal anomalies (Sect. 3.3) and geologically young terrains (Sect. 2.1.2) are key aspects for providing greater insight into possible current activity. Additional evidence of current surface activity could also be found through direct change detection, or indirectly by the identification of fresh features or materials, particularly at small scales. Surface changes might include: albedo or color variability as a function of time; growth or appearance of cracks; increased ridge height or width; lateral changes in offset along a strike-slip faults; change in relative location of chaos blocks; and the presence of new craters. Fresh features might

include regions indicative of surface flows; steep slopes; bright material; areas with anomalous roughness, photometry, or color; and features whose size, albedo, appearance, or cross-cutting relations with other young features indicate very young ages.

Previous searches did not result in any detection of changes over the last few decades. Overlapping images obtained by the Voyager 2 (1979), Galileo (1996–1998), and New Horizons (2007) spacecraft enabled searches for large-scale surface changes over the intervening decades. No detectable surface changes have been found between these datasets despite extensive searches, implying that any current activity must be at a smaller spatial scale, different locations and/or be episodic and not continuous (Phillips et al. 2000; Phillips 2015; Schenk 2020). A maximum surface alteration rate of <1 km²/year, corresponding to a minimum surface age of 30 Myr, was calculated based on the null result found between the Voyager 2 and Galileo images (Phillips et al. 2000). Europa Clipper will provide data over a longer timeframe to continue this search for recent surface activity by identifying changes in comparison with previous imaging datasets. Images from EIS will characterize the surface albedo and color at ≤500-m pixel scale to enable comparisons among previous EIS, Voyager, and Galileo data for assessing large-scale surface changes over the course of decades. Several of the EIS filters were designed to be comparable to their counterparts on Galileo SSI for detailed comparisons which could indicate changes in color and/or albedo over time. Repeat coverage within this dataset will enable assessment of surface changes over the course of the Europa Clipper mission.

Surface albedo can be an indicator of relatively recent activity. The surfaces of airless bodies typically darken with time as they are exposed to the space environment; however, Europa currently defies that general trend. Bright icy material can indicate fresher surfaces, particularly when associated with landforms like steep slopes (i.e., fresh material exposed by mass wasting) or craters (i.e., fresh material excavated from depth and deposited in rays; see Sect. 2.2.3). Dilational band relative albedo varies distinctly with age (Sect. 2.2.2). Thus, relative albedo of surfaces can also be used to identify and characterize recent activity.

Another expected form of current activity is mass wasting. Europa is believed to be covered in regolith (Sect. 2.3). Evidence of mass wasting of that regolith has been found in high-resolution Galileo images, indicating slope processes at this scale may be widespread and ongoing today (Moore et al. 2009). Mapping and quantifying such mass wasting in Europa Clipper data will show the extent of such activity, the driving mechanisms, and material properties of that regolith.

Various instruments will be complementary in the search for fresh material that could indicate current activity. Observations by EIS will allow characterization of small areas of the surface at resolutions of 10- and 1-m/pixel, enabling a search for signs of small-scale resurfacing, weathering, and erosion. Regional-scale images with a resolution of about 25 m/pixel will be sufficient to search for evidence of larger-scale mass wasting. EIS color imaging with pixel scales as small as ∼5 m will be used to identify signs of fresh material based on photometric properties and color ratios. These data will complement MISE data that can be used to map ice grain size and crystallinity, allowing for detection of anomalous surfaces that have experienced recent changes. MISE-derived photometric properties will also constrain the freshness of surface material such as that exposed in downslope mass wasting processes. Young surfaces produced or modified by recent activity are likely to be detectable by E-THEMIS as thermal inertia anomalies (see Sect. 3.3), because their surface textures will not have reached equilibrium due to longer-term surface processes such as sputtering or micrometeorite bombardment. Far-UV spectral albedo maps produced by Europa-UVS will capture both microphysical and chemical composition variations of the uppermost layer of the regolith. This thin veneer can be disturbed by impacts and mass

wasting, replaced or overlain by fresh plume or impact ejecta deposits, and weathered by the intense radiation effects at Europa. Correlating the far-UV measured albedo variations in this thin veneer to thermal anomalies observed by E-THEMIS, chemical compositions detected by SUDA, MASPEX, and MISE as well as topography and subsurface structure measured by EIS and REASON, provides a powerful opportunity to understand the mechanisms driving recent activity.

Detection of subsurface liquid water would also indicate relatively recent activity. As discussed in Sect. 2 and summarized in Fig. 3, a number of the proposed formation mechanisms for various landforms imply the presence of water or brines in Europa's near-surface. As these liquid deposits are expected to be thermodynamically unstable and therefore short-lived, their existence would show that processes are actively reshaping Europa's surface (Steinbrügge et al. 2020a,b). REASON reflectometry measurements will be sensitive to such areas of liquid-bearing porous ice regolith, as they are expected to be present with significantly stronger coherent reflection strengths than those from an area where the regolith pore space is empty (Grima et al. 2016).

In addition to remote sensing, *in situ* measurements will be taken to constrain the frequency and magnitude of current activity by directly measuring materials ejected from the surface during any ongoing events. For example, atmospheric modeling of Europa suggests that geologically young features, such as maculae and chaos terrain, produce signature sputtered compositions (as a ratio to O_2) relative to older, heavily radiolyzed terrain (Teolis et al. 2017). MASPEX will thus measure key chemical species such as CH_4 and HCN that may be sputtered from the surface and identify regions of enhanced ratios that may indicate geologically young features at scales of 35 to 110 km. SUDA will enable direct capture and analysis of any endogenous plume particles and also grains ejected from impacts. In order to constrain the source of detected materials, SUDA will be able to differentiate the background of sputtered material and impact dust ejecta from that of recently erupted plume material that may be derived from the subsurface ocean or other liquid water regions within the ice shell. PIMS measurements of the Jupiter's magnetospheric plasma will determine the surface sputtering rates of Europa and constrain surface weathering (Westlake et al. 2023). PIMS measurements of Europa's ionospheric composition will contribute to our understanding of the surface and the processes that produce the sputtered atmosphere (Becker et al. 2024).

4 Integrated Geologic Dataset(s)

Progress toward answering broader questions of habitability associated with geology will come from the integration of multiple datasets. Each Europa Clipper instrument will generate datasets that can be used to investigate the various aspects of Europa's geology, but as discussed here, the combination of correlated datasets will provide even greater insight. The strength of the instrument suite on Europa Clipper is that it allows this icy world to be interrogated from the subsurface to the space environment, all measurements providing a piece to the puzzle (i.e., sounding the interior to in situ sampling of sputter or ejected material).

With a focus on achieving a comprehensive understanding of the geology of Europa, we provide some examples of key datasets that will be correlated. Compositional data from MISE become more powerful when combined with morphologic and topographic information derived from EIS measurements as it allows us to better understand relations between structures, time stratigraphic units, and any variations in composition. Folding in REASON sounding data provides direct insight as to how the observations on the surface are linked

to subsurface structural or thermal configuration. In relation to the latter, the E-THEMIS dataset also provides complementary information on endogenic thermal features from passive thermal emission while derived maps of thermophysical properties aid in better understanding surface physical properties and their relation to composition.

From its inception, the Europa Clipper flight system has been designed to accommodate an imaging suite covering the wavelength range from 60 nm (UVS) to 33 m (REASON's 9 MHz HF band), and to simultaneously observe along common boresights with overlapping fields of view (Fig. 6 and 7). Its configuration on the spacecraft is intentionally designed to enable the integration of data sets to investigate Europa's habitability. Data from Europa Clipper's instruments cover a substantial swath of the electromagnetic spectrum from the UV (Europa-UVS, EIS), through the visible (EIS), near-infrared (EIS, MISE), mid- and far-infrared (E-THEMIS), and radio (REASON, G/RS) wavelengths, at spatial scales ranging from hemispherical to submeter (Fig. 6). Simultaneously, particles and fields instruments (SUDA, MASPEX, PIMS, ECM, and G/RS) provide crucial information about the local near-surface environment. Table 2 lists key datasets for addressing the broad goals of Europa Clipper's geological investigations. Used together, these datasets will enable Europa's geology to be explored in three-dimensions via a broad swath of the electromagnetic spectrum.

Integration of the various datasets requires the consistent use of agreed upon datums, coordinate systems, map projections, and even data formats (i.e., a spatial data infrastructure (Laura et al. 2018)), and spatial datasets must be geodetically controlled, especially those that are not co-aligned such as MISE and EIS NAC, which can point off-nadir. These considerations have been integrated into the Europa Clipper science and operational strategy from an early stage (Pappalardo et al. 2024; Table 2). Geospatial data will be archived in the Planetary Data System (PDS) in both the IAU east-positive, planetocentric (consistent with the JUICE mission) and west-positive, planetographic coordinate systems.

5 Reconnaissance as feed forward to future exploration

Because of its astrobiological potential, an eventual return to Europa to study this world in situ is a strong desire subsequent to the Europa Clipper mission, and a lander is the next logical step in the exploration of this moon (Hand et al. 2017, 2022; Phillips et al. 2020). Whatever form the next mission to Europa takes, reconnaissance data collected by Europa Clipper will be critical for the identification and assessment of potential future landing sites, which will need to satisfy criteria for both (1) scientific value and (2) landing and operational safety. The top-level requirements of the Europa Clipper investigations (see Table 1 and supplemental material), specifically the geology-related ones, are well-aligned with the needs of reconnaissance. The main inputs to the landing/operational safety aspects of reconnaissance (e.g., measurement of slopes, detection and characterization of boulders and surface roughness) are highly relevant to local-scale surface and regolith characterization (Sect. 2.3).

As a multiple flyby mission, the highest resolution data most relevant for reconnaissance will be collected during the close approach phase (25–100 km altitude) of each flyby. It is likely that one of the approximate 50 regions of closest approach will be the landing site for a future mission. However, not all high-resolution datasets will help address the fundamental needs of a lander and thus not all regions of closest-approach will contain feasible landing sites (Phillips et al. 2023). If the spacecraft remains healthy and resources are available after the prime mission, an extended mission might also provide opportunities
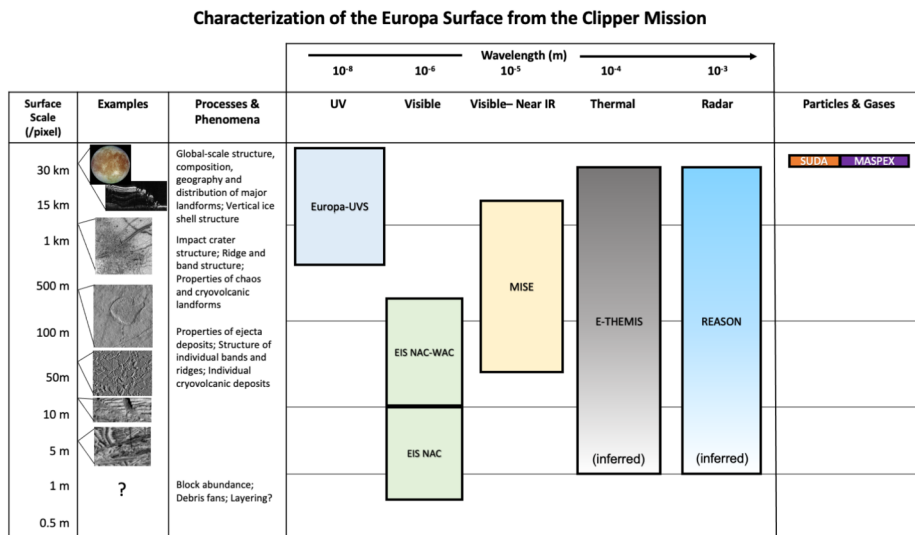
Characterization of the Europa Surface from the Clipper Mission

Wavelength (m): 10^{-8} 10^{-6} 10^{-5} 10^{-4} 10^{-3}

Surface Scale (/pixel)	Examples	Processes & Phenomena	UV	Visible	Visible–Near IR	Thermal	Radar	Particles & Gases
30 km		Global-scale structure, composition, geography and distribution of major landforms; Vertical ice shell structure	Europa-UVS			E-THEMIS	REASON	SUDA MASPEX
15 km								
1 km		Impact crater structure; Ridge and band structure; Properties of chaos and cryovolcanic landforms			MISE			
500 m								
100 m		Properties of ejecta deposits; Structure of individual bands and ridges; Individual cryovolcanic deposits		EIS NAC-WAC				
50m								
10 m								
5 m				EIS NAC		(inferred)	(inferred)	
1 m	?	Block abundance; Debris fans; Layering?						
0.5 m								

Fig. 6 Visualization of how different instruments (colored bars) on Europa Clipper will observe Europa's surface at a variety of scales (left). The gradation at the bottom of the E-THEMIS and REASON bars indicates that the meter-scale is inferred by the data these instruments take (rather than directly observed). The in-situ instruments MASPEX and SUDA (far right bars) will provide observations of Europa at the 30-km scale and are therefore included in this visualization even though they do not provide observations at a particular wavelength like the other, remote sensing instruments.

for targeted, follow-on observations of potential landing sites. See Phillips et al. (2023) for a full discussion of the reconnaissance strategy for landing on Europa.

5.1 Scientific value of potential landing sites

The ability to sample below the surface would enable a lander mission to expand upon the science return from the Europa Clipper mission. The goals of a future landed mission, such as to search for biosignatures and assess the geochemical and geophysical context (Hand et al. 2022), will guide the selection of potential landing sites. As such, sites with lower radiation processing will be preferred because they are predicted to have a greater likelihood of preserving intact biological signatures closer to the surface (Hand et al. 2017; Nordheim et al. 2018). Sites that are thought to contain ocean-derived materials would also be important. Also of interest are areas shown to have signs of current or recent activity (e.g., color changes, morphological changes (Sect. 3.3), plumes (Sect. 3.1), or cryovolcanic deposits). In addition, sites of thermal anomalies (Sect. 3.2) or places where radar observations suggest the presence of shallow subsurface liquid water would be compelling targets of interest.

5.2 Landing and operational safety constraints for potential landing sites

Fundamental to any landed asset is the ability to safely deliver the flight system to the ground. To accomplish this at Europa will require assessments of local surface properties such as slope (e.g., <25°; Hand et al. 2022), surface roughness, vertical topographic relief (e.g., <1 m; Hand et al. 2022), and block abundance. Slope information derived from Galileo data suggests that any lander should require robustness to slopes greater than 15°
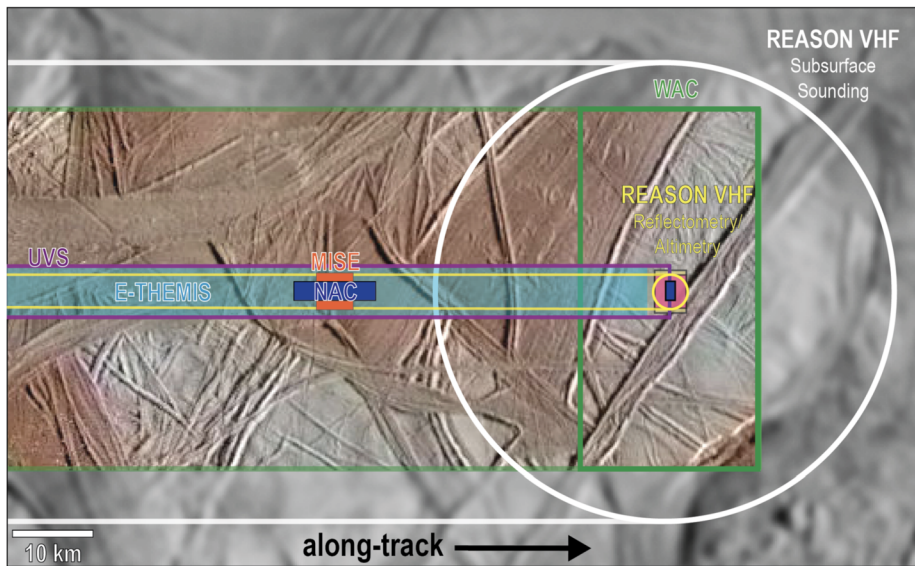
Fig. 7 Approximate field of view (FOV) for each of the Europa Clipper remote sensing instruments, evaluated at 100 km altitude as an example. FOVs are shown for the EIS NAC (blue; 1 m/pixel resolution at this altitude), EIS WAC (green; 22 m/pixel), Europa-UVS (purple; 35 m/pixel), E-THEMIS (cyan; 250 m/pixel), MISE (pink; 25 m/pixel), and REASON (white) instruments. Colors of instrument FOVs correspond to label colors. REASON FOVs show the area of the surface that contributes to a single echo measurement and so are essentially the surface spatial resolutions of these types of measurements. The yellow circle ($\sim$ 3.4 km in diameter) represents the area on the surface that contributes to an individual reflection to REASON VHF altimetry and reflectometry measurements. The white circle ($\sim$ 66 km in diameter) encompasses the area on the surface that may reflect radar energy arriving at the REASON antennas at the same time as a reflection recorded during the subsurface sounding of a target at 3 km depth in the ice shell. Bolded shapes on the right portion of the illustration comprise FOVs for individual instrument observations (although at this altitude EIS WAC will be used in pushbroom mode only, a representative footprint for framing mode is shown for comparison), while the partially transparent colored strips on the left portion of the image illustrate push broom dataset coverage when integrated along-track during a Europa flyby. Background images: Galileo PIA23872 (color, 223 m/pixel; grayscale is same image blurred for illustrative purposes).

(Schenk 2009). It must also be noted that slopes smaller than $\sim$40-m-scale are unknown and could be higher. Images acquired by EIS along with derived Digital Terrain Models (DTMs) will be used to determine slopes, topographic variations, block heights, and fracture hazards. In addition, thermal inertia derived from E-THEMIS data can be used to broadly characterize the safety of potential landing sites as it informs on the cohesiveness and porosity of the material along with providing insight as to the roughness of the surface (Christensen et al. 2024). In an independent manner, REASON data will inform on the porosity and cohesiveness of the surface and near subsurface and can be used to characterize the surface roughness at horizontal scales of 5 m and 33 m (Blankenship et al. 2024, this collection).

    A technique that has proven effective at Mars and at the asteroid Bennu (Nelessen et al. 2019; Lauretta et al. 2022 and references therein) in guiding a lander to its destination on the surface is Terrain Relative Navigation (TRN), which uses onboard processing of real-time imaging to guide the final descent. It is anticipated that such a technique will be used for a Europa lander during the deorbit, descent, and landing process to localize the spacecraft and precisely navigate to the planned landing site. To make this feasible, local-scale EIS data would enable a small landing ellipse $\sim$200 m across, while stereo images obtained at

Table 2 The global, regional, and local scale datasets from each Europa Clipper instrument that will be used to investigate Europa's geology. Note these terms are not formally defined at the same spatial scales for all instruments, but this table summarizes how datasets will address the formation hypotheses and processes discussed in Sect. 2 at different spatial scales. Coverage, resolution, etc. values are based on measurement requirements and Planning Guidelines; values achieved during the active mission may be an improvement on these.

Data Type	Global Scale	Regional Scale	Local Scale
Global Shape	• REASON altimetry (∼15 m vertical precision 1600 km long globally distributed profiles) • Europa-UVS occultations (∼1 m vertical accuracy) • EIS limb profiles (∼100 m vertical accuracy) • Gravity/Radio Science	NA	NA
Mapping and Morphology	• EIS WAC NAC Photomosaic (≥80% coverage at ≤100 m/pixel) • EIS NAC color mosaic (≥3 filters at 250–400 m/pixel) • EIS WAC NAC topography (≥30% coverage at ≤100 m/posting, 50 m vertical precision) • REASON altimetry (2 km along track, ∼15 m vertical precision >30,000 km cumulative ground track length)	• EIS WAC NAC (≥5% of the surface, with a target of ≥30% at 25 m/pixel) • EIS WAC NAC topography (target of ≥1.7% coverage) • REASON altimetry (2 km along track, 15 m vertical precision, up to three 800 km long profiles in mapped panels)	• EIS NAC images (≥ 40 sites at ≤1 m/pixel, and ≥20 sites at ≤10 m/pixel) • EIS NAC topography (≥40 sites with 1 m postings and vertical resolution ∼0.5 m)
Composition (see also Becker et al. 2024)	• MISE hyperspectral data (0.8–5 μm, ≥70% global coverage at 10 km/pixel) • Europa-UVS (54 nm – 0.21 μm, 70% coverage at 100 km/pixel) • SUDA and MASPEX (in situ at close approach) • EIS NAC color mosaic (≥3 filters at 250–400 m/pixel) ≥25% at ≤100 m/pixel	• MISE hyperspectral data (≥0.3% coverage at < 300 m/pixel) • Europa-UVS (54 nm – 0.21 μm at ∼1 km/pixel retrieved at spacecraft altitudes <1000 km) • SUDA and MASPEX (in situ at close approach, regional spatial resolution ≥ flyby altitude) • EIS color (∼3% at ≤25 m/pixel)	MISE local hyperspectral data at ≥14 globally distributed sites, down to 25 m/pixel at 100 km and 7.5 m/pixel at 25 km altitude • EIS small scale color (≥10 sites at ≤10 m/pixel)

≤22 m/pixel scale would cover the area surrounding the landing site by ≥22 km on all sides (see Fig. 7 for comparison of Europa Clipper instruments' FOVs). Because of the small size of the landing ellipse, the number of potential sites within an imaged area could be large, increasing the odds of finding landing areas that have high science value and are also safe from an engineering perspective (Johnson et al. 2015).

Table 2 (*Continued*)

Data Type	Global Scale	Regional Scale	Local Scale
Thermophysical Surface Properties	• Europa-UVS (54 nm – 0.21 μm, 70% coverage at 100 km/pixel) • E-THEMIS (80% coverage with 50% day/night overlap at 25 km/pixel) • REASON reflectometry (11 of 14 mapped panels) • MISE hyperspectral data (0.8–4.8 μm, ≥70% global coverage at 10 km/pixel) to constrain ice grain size and porosity as a function of depth down to ~1 cm and temperature from ice band positions	• E-THEMIS (18 distinct sites separated by a distance of 100 km, dayside and nightside, observation of 15+ unique sites at 250 m/pixel (3+ anti-Jovian and 3+ sub-Jovian sites) • Europa-UVS (54 nm – 0.21 μm at ~1 km/pixel retrieved at spacecraft altitudes <1000 km • REASON reflectometry (up to three 800 km long profiles in each mapped panel) • MISE hyperspectral data (≥0.3% coverage at < 300 m/pixel) to constrain ice grain size and porosity as a function of depth down to ~1 cm and temperature from ice band positions	• REASON reflectometry (cm-m scale roughness at >10 km scale resolution and permittivity (with additional compositional constraints provides density) • E-THEMIS (two bands 7–14 μm and 28+ to derive meter-scale block abundance globally) • EIS Photometry (local scale properties derived from 500 m/pixel images at 2 sites at 6 different phase angles) • MISE hyperspectral data (≥14 globally distributed sites at < 50 m/pixel) to constrain ice grain size and porosity as a function of depth down to ~1 cm and temperature from ice band positions
Thermal Anomalies and Current Geologic Activity	• E-THEMIS (80% coverage at 25 km/pixel, with 2 K accuracy and precision) • MISE 4.5–5 μm data to map thermal anomalies (3.6 km diameter and >190 K) • EIS plume searches (terminator and limb observations at distributed longitudes, true anomalies and high phase angles at ≤10 km/pixel) • MASPEX global atmospheric detection of plume activity	• EIS recent activity dataset (500 m/pixel color images overlapping previous mission coverage) • REASON plume identification (between 35 km and 1000 km spacecraft altitude) • MISE 4.5–5 μm data to map thermal anomalies (>110 m diameter and >190 K)	• E-THEMIS 250 m/pixel or better • MISE 4.5–5 μm data to map thermal anomalies (>18 m diameter and >190 K) • REASON mapping of plume outfall • EIS high-resolution (<10 m/pixel) images (as discussed in Sec 2.3)
Subsurface Structure	• REASON HF and VHF sounding (11 of 14 mapped panels) • G/RS Line-of-Sight Doppler residuals (resolution comparable to S/C altitude above surface)	• REASON HF and VHF shallow sounding (up to three 800 km long profiles in mapped panels)	• E-THEMIS surficial layering (18 distinct sites separated by a distance of 100 km, dayside and nightside, observation of 15+ unique sites at 250 m/pixel) • EIS images that reveal layering or regional variations in impact crater morphologies

While the collection of reconnaissance data to select a landing site is not a requirement of the Europa Clipper mission, a set of Planning Guidelines have been developed. These describe the fundamental parameters needed (e.g., image resolution, stereo imaging constraints, and site illumination) (Phillips et al. 2023).

6 Summary

The existing data of Europa, primarily sourced from Voyager, Galileo, and ground-based observations, have revealed this icy world to be potentially one of the most active and astrobiologically compelling targets in the solar system. The Europa Clipper mission will dramatically improve upon these existing datasets, with orders of magnitude improvements in spatial coverage, image and spectral resolution and with coordinated multi-instrument remote sensing and in situ observations. Europa's geology will be investigated at spatial scales from the global (kilometers) to the local (meter-scale), in wavelengths from the UV to the near-IR, thermal, and radio. Measurements of particles and fields will also contribute to our understanding of this complex moon and its geologic history.

The knowledge gained through addressing open questions about Europa's geology, feature formation, and potential recent activity, will contribute to Europa Clipper's overarching goal of assessing whether or not Europa harbors a habitable environment. Investigation of the geology will provide insight into (1) the connection between any liquid subsurface water and surface features, (2) recent activity, and/or young surface age, (3) the degree that this moon is active, (4) the depth to an extant liquid ocean and/or subsurface water bodies, and (5) the energy required for a habitable environment. If geologic features also contain signatures of salts, organics, reductants, or other compounds indicative of water-rock reactions, then the chemistries conducive to a habitable environment could be present (Becker et al. 2024). Additionally, if evidence is discovered of subsumption, resurfacing, or missing terrains, then exchange of material between the surface and the subsurface may be occurring. The resulting mixing of oxidants and reductants could provide a habitable subsurface environment (Vance et al. 2023). Understanding Europa's geologic features, their formation, and any recent activity are key inputs in constraining Europa's habitability. Further, in constraining the degree to which Europa possesses the components for habitability, as evidenced through its geology, the Europa Clipper mission will provide examples and comparisons for application at other ocean worlds, so that we can better understand why some bodies form habitable environments and others do not.

Acronyms

DEM	Digital Elevation Model
DTM	Digital Terrain Model
ECM	Europa Clipper Magnetometer
EIS	Europa Imaging System
E-THEMIS	Europa Thermal Emission Imaging System
Europa-UVS	Europa Ultraviolet Spectrograph
FG	Focus Group
G/RS	Gravity and Radio Science
GWG	Geology Working Group

HDA	Hazard Detection and Avoidance
IR	Infrared
LIDAR	LIght Detection And Ranging
MASPEX	MAss SPectrometer for Planetary EXploration/Europa
MISE	Mapping Imaging Spectrometer for Europa
MRL	Map Relative Localization
NAC	Narrow Angle Camera
PIMS	Plasma Instrument for Magnetic Sounding
PPR	Photopolarimeter-Radiometer on the Galileo spacecraft
PSG	Project Science Group
REASON	Radar for Europa Assessment and Sounding: Ocean to Near-surface
SUDA	SUrface Dust Mass Analyzer
TRN	Terrain-relative Navigation
TWG	Thematic Working Group
UV	Ultraviolet
WAC	Wide Angle Camera

Declarations

Competing Interests The authors have no conflicts of interest to disclose.

References

Abramov O, Spencer JR (2008) Numerical modeling of endogenic thermal anomalies on Europa. Icarus 195:378–385

Abramov O et al (2013) Detectability of thermal signatures associated with active formation of 'chaos terrain' on Europa. EPSL 384:37–41

Aglyamov Y, Schroeder DM, Vance SD (2017) Bright prospects for radar detection of Europa's ocean. Icarus 281:334–337. https://doi.org/10.1016/j.icarus.2016.08.014

Arnold H, Liuzzo L, Simon S (2019) Magnetic signatures of a plume at Europa during the Galileo E26 flyby. Geophys Res Lett 46:1149–1157. https://doi.org/10.1029/2018GL081544

Aydin A (2006) Failure modes of the lineaments on Jupiter's moon, Europa: implications for the evolution of its icy crust. J Struct Geol 28:2222–2236

Becker TM et al (2024) Exploring the composition of Europa with the upcoming Europa Clipper mission. Space Sci Rev 220

Berg JJ, Goldstein DB, Varghese PL, Trafton LM (2016) DSMC simulation of Europa water vapor plumes. Icarus 277:370–380

Bierhaus EB, Schenk PM (2010) Constraints on Europa's surface properties from primary and secondary crater morphology. J Geophys Res 115:E12004. https://doi.org/10.1029/2009JE003451

Bierhaus EB et al (2001) Pwyll secondaries and other small craters on Europa. Icarus 153:264–276. https://doi.org/10.1006/icar.2001.6690

Bierhaus EB, Chapman CR, Merline WJ (2005) Secondary craters on Europa and implications for cratered surfaces. Nature 437(7062):1125–1127. https://doi.org/10.1038/nature04069

Bierhaus EB, Zahnle K, Chapman CR, Pappalardo RT, McKinnon WR, Khurana KK (2009) Europa's crater distributions and surface ages. In: Pappalardo RT, McKinnon WB, Khurana KK (eds) Europa. p 161. University of Arizona Press, Tucson

Black GJ, Campbell DB, Nicholson PD (2001) Icy Galilean satellites: modeling radar reflectivities as a coherent backscatter effect. Icarus 151(2):167–180. https://doi.org/10.1006/icar.2001.6616

Bland MT, McKinnon WB (2012) Forming Europa's folds: strain requirements for the production of large-amplitude deformation. Icarus 221(2):694–709. https://doi.org/10.1016/j.icarus.2012.08.029

Bland MT, McKinnon WB (2013) Does folding accommodate Europa's contractional strain? The effect of surface temperature on fold formation in ice lithospheres. Geophys Res Lett 40:2534–2538. https://doi.org/10.1002/grl.50506

Blaney DL et al (2024) The Mapping Imaging Spectrometer for Europa (MISE). Space Sci Rev 220

Blankenship DD, Young DA, Moore WB, Moore JC (2009) Radar sounding of Europa's subsurface properties and processes: the view from Earth. In: Pappalardo RT, McKinnon WB, Khurana KK (eds) Europa. University of Arizona Press, Tucson, pp 631–654. ISBN 9780816528448

Blankenship DD et al (2024) Radar for Europa Assessment and Sounding: Ocean to Near-surface (REASON). Space Sci Rev 220

Bramson AM, Phillips CB, Emery JP (2011) A search for ongoing geologic activity on Jupiter's satellites. In: 42nd Lunar and Planetary Science Conference. Abstract #1606

Breer BR et al (2019) Energetic ion dynamics in the perturbed electromagnetic fields near Europa. J Geophys Res 124

Buck WR, Lavier LL, Poliakov ANB (2005) Modes of faulting at mid-ocean ridges. Nature 434:719–723

Buffo JJ, Schmidt BE, Huber C, Walker CC (2020) Entrainment and dynamics of ocean-derived impurities within Europa's ice shell. J Geophys Res, Planets. https://doi.org/10.1029/2020JE006394

Carr MH, Belton MJS, Chapman CR, Davies ME, Geissler P, Greenberg R et al (1998) Evidence for a subsurface ocean on Europa. Nature 391(6665):363–365. https://doi.org/10.1038/34857

Carter SP, Blankenship DD, Peters ME, Young DA, Holt JW, Morse DL (2007) Radar-based subglacial lake classification in Antarctica. Geochem Geophys Geosyst 8(3). https://doi.org/10.1029/2006GC001408

Chan K, Grima C, Rutishauser A, Young DA, Culberg R, Blankenship DD (2023) Spatial characterization of near-surface structure and meltwater runoff conditions across the Devon Ice Cap from dual-frequency radar reflectivity. Cryosphere 17:1839–1852. https://doi.org/10.5194/tc-17-1839-2023. 2023

Chivers CJ, Buffo JJ, Schmidt BE (2021) Thermal and chemical evolution of small, shallow water bodies in Europa's ice shell. J Geophys Res, Planets. https://doi.org/10.1029/2020JE006692

Christensen PR et al (2024) The Europa Thermal Emission Imaging System (E-THEMIS) investigation for the Europa Clipper mission. Space Sci Rev 220

Collins G, Nimmo F (2009) Chaotic terrain on Europa. In: Pappalardo RT, McKinnon WB, Khurana KK (eds) Europa. University of Arizona Press, Tucson, pp 259–281

Collins GC, Head JW, Pappalardo RT, Spaun NA (2000) Evaluation of models for the formation of chaotic terrain on Europa. J Geophys Res, Planets 105(E1):1709–1716. https://doi.org/10.1029/1999JE001143

Collins GC, Patterson GW, Detelich CE, Prockter LM, Kattenhorn SA, Cooper CM, Rhoden AR, Cutler BB, Oldrid SR, Perkins R, Rezza CA (2022) Episodic plate tectonics on Europa: evidence for widespread patches of mobile-lid behavior in the anti-Jovian hemisphere. J Geophys Res 127:e2022JE007492. https://doi.org/10.1029/2022JE007492

Cook AF, Shoemaker EM, Soderblom LA, Mullins KF, Fielder R (1982) Volcanism in ice on Europa. Bull Am Astron Soc 14:736–737

Cook AF, Shoemaker EM, Soderblom LA, Mullins KF, Fielder R (1983) Volcanism in Ice on Europa. Report on the Planetary Geology Program 1982, NASA Technical Memorandum, TM-85127, 415–416

Corr HFJ, Doake CSM, Jenkins A, Vaughan DG (2001) Investigations of an "ice plain" in the mouth of Pine iSland Glacier, Antarctica. J Glaciol 47(156):7. https://doi.org/10.3189/172756501781832395

Coulter CE (2009) Kinematic and morphological evolution of Europa's ridges. PhD thesis, University of Idaho

Coulter CE, Kattenhorn SA (2010) The morphology of Europa's ridges examined in a detailed topographic and kinematic survey. In: AGU fall meeting abstracts, Vol. 2010, pp P21B-1599

Cox R, Bauer AW (2015) Impact breaching of Europa's ice: constraints from numerical modeling. J Geophys Res Planets 120:1708–1719

Cox R, Ong LCF, Arakawa M, Scheider KC (2008) Impact penetration of Europa's ice crust as a mechanism for formation of chaos terrain. Meteorit Planet Sci 43(12):2027–2048

Craft KL et al (2016) Fracturing and flow: investigations on the formation of shallow water sills on Europa. Icarus 274:297–313. https://doi.org/10.1016/j.icarus.2016.01.023

Craft KL, Walker C, Quick L, Lowell R (2019) Freckles, spots, and domes on Europa and Ceres: Surface features driven by subsurface cryovolcanic diking and surface response? 50th Lunar and Planetary Science Conference. Abstract #3102

Crawford GD, Stevenson DJ (1988) Gas-driven water volcanism and the resurfacing of Europa. Icarus 73:66–79

Culberg R, Schroeder DM, Steinbrügge G (2022) Double ridge formation over shallow water sills. Nat Commun 13:2007

Culha C, Manga M (2016) Geometry and spatial distribution of lenticulae on Europa. Icarus 271:49–56. https://doi.org/10.1016/j.icarus.2015.12.052

Culha C et al (2020) Assessing the detectability of Europa's eutectic zone using radar sounding. Icarus 339:113578. https://doi.org/10.1016/j.icarus.2019.113578

Dalton JB III, Shirley JH, Kamp LW (2012) Europa's icy bright plains and dark linea: exogenic andendogenic contributions to composition and surface properties. J Geophys Res 117:E03003. https://doi.org/10.1029/2011JE003909

Davies AG (2007) Volcanic plumes. In: Volcanism on Io – a comparison with Earth. Cambridge University Press, Cambridge, UK, pp 253–268

Doggett T, Greeley R, Figueredo P (2009) Geologic stratigraphy and evolution of Europa's surface. In: Pappalardo RT, McKinnon WB, Khurana KK (eds) Europa. University of Arizona Press, Tucson, pp 137–159

Dombard AJ, Patterson GW, Lederer AP, Prockter LM (2013) Flanking fractures and the formation of double ridges on Europa. Icarus 223:74–81

Domingue D, Verbiscer A (1997) Re-analysis of the solar phase curves of the icy Galilean satellites. Icarus 128:49–74. https://doi.org/10.1006/icar.1997.5730

Escartín J, Cowie PA, Searle RC, Allerton S, Mitchell NC, MacLeod CJ, Slootweg AP (1999) Quantifying tectonic strain and magmatic accretion at a slow spreading ridge segment, mid-Atlantic ridge, 29°N. J Geophys Res 104:10,421–10,437

Fagents SA et al (2000) Cryomagmatic mechanisms for the formation of Rhadamanthys Linea, triple band margins, and other low-albedo features on Europa. Icarus 144:54–88

Fagents SA (2003) Considerations for effusive cryovolcanism on Europa: the post-Galileo perspective. J Geophys Res 108:5139. https://doi.org/10.1029/2003JE002128

Figueredo PH, Greeley R (2000) Geologic mapping of the northern leading hemisphere of Europa from Galileo solid-state imaging data. J Geophys Res, Planets 105:22629–22646

Figueredo PH, Greeley R (2004) Resurfacing history of Europa from pole-to-pole geological mapping. Icarus 167(2):287–312

Figueredo PH, Chuang FC, Rathbun J, Kirk RL, Greeley R (2002) Geology and origin of Europa's "Mitten" feature (Murias Chaos). J Geophys Res 107(E5). https://doi.org/10.1029/2001JE001591

Gaidos EJ, Nimmo F (2000) Tectonics and water on Europa. Nature 405(6787):637–637

Geissler PE, Greenberg R, Hoppa G, McEwen A, Tufts R, Phillips C, Clark B, Ockert-Bell M, Helfenstein P, Burns J, Veverka J, Sullivan R, Greeley R, Pappalardo RT, Head JW, Belton MJS, Denk T (1998) Evolution of lineaments on Europa: clues from Galileo multispectral imaging observations. Icarus 135:107–126

Giono G, Roth L, Ivchenko N, Saur J, Retherford K, Schlegel S, Ackland M, Strobel D (2020) An analysis of the statistics and systematics of limb anomaly detections in HST/STIS transit images of Europa. Astron J 159:155

Goodman JC, Collins GC, Marshall J, Pierrehumbert RT (2004) Hydrothermal plume dynamics on Europa: implications for chaos formation. J Geophys Res 109:E03008. https://doi.org/10.1029/2003JE002073

Greeley R, Sullivan R, Bender KC, Homan KS, Fagents SA, Pappalardo RT, Head JW, the Galileo SSI Team (1997) Europa triple bands: Galileo images. In: 28th Lunar and Planetary Science Conference, pp 455–456. [Abstract]

Greeley R et al (1998) Europa: initial Galileo geological observations. Icarus 135:4–24

Greeley R, Figueredo PH, Williams DA, Chuang FC, Klemaszewski JE, Kadel SD, Prockter LM, Pappalardo RT, Head JW, Collins GC, Spaun NA, Sullivan RJ, Moore JM, Senske DA, Tufts BR, Johnson TV, Belton MJS, Tanaka KL (2000) Geologic mapping of Europa. J Geophys Res, Planets 105:22559–22578

Greeley R, Chyba CF, Head JW, McCord T, McKinnon WB, Pappalardo RT, Figueredo PH (2004) Geology of Europa. In: Bagenal F, Dowling TE, McKinnon WB (eds) Jupiter. The planet, satellites and magnetosphere. Cambridge University Press, pp 329–362

Greenberg R (2004) The evil twin of agenor: tectonic convergence on Europa. Icarus 167(2):313–319

Greenberg R, Geissler P, Hoppa G, Tufts BR, Durda DD, Pappalardo RT, Head JW, Greeley R, Sullivan R, Carr MH (1998) Tectonic processes on Europa: tidal stresses, mechanical response, and visible features. Icarus 135:64–78

Greenberg R, Hoppa GV, Tufts BR, Geissler P, Riley J (1999) Chaos on Europa. Icarus 141:263–286

Greenberg R, Leake MA, Hoppa GV, Tufts BR (2003) Pits and uplifts on Europa. Icarus 161(1):102–126

Grima C, Blankenship DD, Young DA, Schroeder DM (2014b) Surface slope control on firn density at Thwaites Glacier, West Antarctica: results from airborne radar sounding. Geophys Res Lett 41(19):6787–6794. https://doi.org/10.1002/2014GL061635

Grima C, Schroeder DM, Blankenship DD, Young DA (2014a) Planetary landing-zone reconnaissance using ice-penetrating radar data: concept validation in Antarctica. Planet Space Sci 103:191–204. https://doi.org/10.1016/j.pss.2014.07.018

Grima C, Blankenship DD, Schroeder DM (2015) Radar signal propagation through the ionosphere of Europa. Planet Space Sci 117:421–428. https://doi.org/10.1016/j.pss.2015.08.017

Grima C, Greenbaum JS, Lopez Garcia EJ, Soderlund KM, Rosales A, Blankenship DD, Young DA (2016) Radar detection of the brine extent at McMurdo Ice Shelf, Antarctica, and its control by snow accumulation. Geophys Res Lett 43(13):7011–7018. https://doi.org/10.1002/2016GL069524

Grima C, Mastrogiuseppe M, Hayes AG, Wall SD, Lorenz RD, Hofgartner JD et al (2017) Surface roughness of Titan's hydrocarbon seas. Earth Planet Sci Lett 474:20–24. https://doi.org/10.1016/j.epsl.2017.06.007

Groenleer JM, Kattenhorn SA (2008) Cycloid crack sequences on Europa: relationship to stress history and constraints on growth mechanics based on cusp angles. Icarus 193:158–181. https://doi.org/10.1016/j.icarus.2007.08.032

Han L, Melosh HJ (2010) Origin of Europa's ridges by incremental ice-wedging. In: AGU Fall Meeting 2010. Abstr. #P33B-1577

Han L, Showman AP (2008) Implications of shear heating and fracture zones for ridge formation on Europa. Geophys Res Lett 35

Hand KP, Chyba CF, Carlson RW, Cooper JF (2006) Clathrate hydrates of oxidants in the ice shell of Europa. Astrobiology 6(3):463–482

Hand KP et al (2017) Report of the Europa Lander Science Definition Team. National Aeronautics and Space Administration

Hand KP et al (2022) Science goals and mission architecture of the Europa lander mission concept. Planet Sci J 3:22. https://doi.org/10.3847/PSJ/ac4493

Hanel R et al (1979) Infrared observations of the Jovian system from Voyager 2. Science 206(4421):952–956

Hansen OL (1973) Ten-micron eclipse observations of Io, Europa, and Ganymede. Icarus 18(2):237–246. https://doi.org/10.1016/0019-1035(73)90208-X

Hansen CJ, Esposito LW, Hendrix AR (2019) Ultraviolet observation of Enceladus' plume in transit across Saturn, compared to Europa. Icarus 330:256–260

Head JW, Pappalardo RT (1999) Brine mobilization during lithospheric heating on Europa: implications for formation of chaos terrain, lenticula texture, and color variations. J Geophys Res, Planets 104(E11):27143–27155. https://doi.org/10.1029/1999JE001062

Head JW, Pappalardo RT, Sullivan R (1999) Europa: morphological characteristics of ridges and triple bands from Galileo data (E4 and E6) and assessment of a linear diapirism model. J Geophys Res, Planets 104:24223–24236

Helfenstein P, Cook AF (1984) Active venting on Europa?: analysis of a transient bright surface feature. In: Lunar and planetary science conference XV, pp 354–355

Helfenstein P et al (1998) Galileo observations of Europa's opposition effect. Icarus 135(1):41–63

Hendrix AR, Domingue DL, King K (2005) The icy Galilean satellites: ultraviolet phase curve analysis. Icarus 173(1):29–49. https://doi.org/10.1016/j.icarus.2004.06.017

Hoppa GV, Greenberg R, Tufts BR, Geissler PE (1999a) Plume detection on Europa: locations of favorable tidal stress. In: Lunar and planetary science conference XXX, Abstract 1603

Hoppa G, Tufts BR, Greenberg R, Geissler P (1999b) Strike–slip faults on Europa: global shear patterns driven by tidal stress. Icarus 141:287–298. https://doi.org/10.1006/icar.1999.6185

Hoppa GV, Tufts BR, Greenberg R, Geissler P (1999c) Formation of cycloidal features on Europa. Science 285:1899–1902

Hoppa GV, Greenberg R, Riley J, Tufts BR (2001a) Observational selection effects in Europa image data: identification of chaotic terrain. Icarus 151(2):181–189. https://doi.org/10.1006/icar.2000.6571

Hoppa GV, Tufts BR, Greenberg R, Hurford TA, O'Brien DP, Geissler PE (2001b) Europa's rate of rotation derived from the tectonic sequence in the Astypalaea region. Icarus 153(1):208–213

Hoyer L, Kattenhorn SA, Watkeys MK (2014) Multistage evolution and variable motion history of Agenor Linea, Europa. Icarus 232:60–80. https://doi.org/10.1016/j.icarus.2013.12.010

Howell SM, Pappalardo RT (2018) Band formation and ocean-surface interaction on Europa and Ganymede. Geophys Res Lett 45(10):4701–4709

Howell SM, Ito G, Behn MD, Martinez F, Olive JA, Escartín J (2016) Magmatic and tectonic extension at the Chile ridge: evidence for mantle controls on ridge segmentation. Geochem Geophys Geosyst 17(6):2354–2373

Howell SM, Olive JA, Ito G, Behn MD, Escartin J, Kaus B (2019) Seafloor expression of oceanic detachment faulting reflects gradients in mid-ocean ridge magma supply. Earth Planet Sci Lett 516:176–189

Howell S et al (2021) Formation of Europas chaotic terrains by porosity compaction without the presence of liquid water. AGU Fall Meeting Abstracts 2021:P51C-04. https://ui.adsabs.harvard.edu/abs/2021AGUFM.P51C..04H/abstract

Hurford TA, Beyer RA, Schmidt B, Preblich B, Sarid AR, Greenberg R (2005) Flexure of Europa's lithosphere due to ridge-loading. Icarus 177:380–396

Hurford TA, Sarid AR, Greenberg R (2007) Cycloidal cracks on Europa: improved modeling and non-synchronous rotation implications. Icarus 186(1):218–233

Hurford TA, Sarid AR, Greenberg R, Bills BG (2009) The influence of obliquity on Europan cycloid formation. Icarus 202(1):197–215

Jia X, Kivelson MG, Khurana KK, Kurth W et al (2018) Evidence of a plume on Europa from Galileo magnetic and plasma wave signatures. Nat Astron 2:459–464. https://doi.org/10.1038/s41550-018-0450-z

Jia X, Kivelson MG, Paranicas C (2021) Comment on "An active plume eruption on Europa during Galileo flyby E26 as indicated by energetic proton depletions" by Huybrighs et al. Geophys Res Lett 48:e2020GL091550. https://doi.org/10.1029/2020GL091550

Johnson TV, Pilcher CB (1977) Satellite spectrophotometry and surface compositions. In: Burns JA (ed) Planetary satellites, pp 232–268. University of Arizona Press, Tucson

Johnson TV, Morrison D, Matson DL, Veeder GJ, Brown RH, Nelson RM (1984) Io volcanic hotspots: stability and longitudinal distribution. Science 226:134–137

Johnson AE, Cheng Y, Montgomery JF, Trawny N, Tweddle B, Zheng JX (2015) Real-time terrain relative navigation test results from a relevant environment for Mars landing. In: AIAA guidance, navigation, and control conference, 5–9 January 2015, Kissimmee, Florida

Johnston SA, Montési LGJ (2014) Formation of ridges on Europa above crystallizing water bodies inside the ice shell. Icarus 237:190–201

Kadel SD, Fagents SA, Greeley R (1998) Trough-bounding ridge pairs on Europa – considerations for an endogenic model of formation. In: Proceedings of the lunar and planetary science conference XXIX. Abstract 1078

Kadel SD et al (2000) Geological history of the Tyre region of Europa: a regional perspective on Europan surface features and ice thickness. J Geophys Res 105:22657–22670. https://doi.org/10.1029/1999JE001203

Kalousová K et al (2014) Ice melting and downward transport of meltwater by two-phase flow in Europa's ice shell. J Geophys Res, Planets 119(3):532–549

Kapitsa AP, Ridley JK, Robin G. de Q., Siegert MJ, Zotikov IA (1996) A large deep freshwater lake beneath the ice of central East Antarctica. Nature 381(6584):684–686. https://doi.org/10.1038/381684a0

Kattenhorn SA (2002) Nonsynchronous rotation evidence and fracture history in the bright plains region, Europa. Icarus 157:490–506

Kattenhorn SA (2004) Strike-slip fault evolution on Europa: evidence from tailcrack geometries. Icarus 172(2):582–602

Kattenhorn S, Hurford T (2009) Tectonics of Europa. In: Pappalardo RT, McKinnon WB, Khurana KK (eds) Europa. University of Arizona Press, Tucson, pp 199–236

Kattenhorn SA, Prockter LM (2014) Evidence for subduction in the ice shell of Europa. Nat Geosci 7:762–767

Kempf S et al (2024) SUDA: a SUrface Dust Analyser for compositional mapping of the Galilean moon Europa. Space Sci Rev 220

Kieffer SW, Lu X, Bethke CM, Spencer JR, Marshak S, Navrotsky A (2006) A clathrate reservoir hypothesis for Enceladus' south polar plume. Science 314(5806):1764–1766

Kivelson MG, Jia X, Lee KA et al (2023) The Europa Clipper Magnetometer. Space Sci Rev 219:48. https://doi.org/10.1007/s11214-023-00989-5

Laura JR et al (2018) Framework for the development of planetary spatial data infrastructures: a Europa case study. Earth and Space Science 5:486–502. https://doi.org/10.1029/2018EA000411

Lauretta DS et al (2022) Spacecraft sample collection and subsurface excavation of asteroid (101955) Bennu. Science 377:285–291. https://doi.org/10.1126/science.abm1018

Lee S, Pappalardo RT, Makris NC (2005) Mechanics of tidally driven fractures in Europa's ice shell. Icarus 177:367–379. https://doi.org/10.1016/j.icarus.2005.07.003

Leonard EJ, Pappalardo RT, Yin A (2018a) Analysis of very-high-resolution Galileo images and implications for resurfacing mechanisms on Europa. Icarus 312:100–120. https://doi.org/10.1016/j.icarus.2018.04.016

Leonard EJ, Patthoff DA, Senske DA (2018b) The global geologic map of Europa at 1:15 M. United States Geologic Survey

Leonard EJ, Yin A, Pappalardo RT (2020) Ridged plains on Europa reveal a compressive past. Icarus 343:113709

Leonard E, Patthoff DA, Senske D (2023) Global geologic map of Europa: U.S. Geological Survey Scientific Investigations Map 3513, scale 1:15,000,000, pamphlet 18 p. https://doi.org/10.3133/sim3513

Lichtenberg KA, McKinnon WB, Barr AC (2006) Heat flux from impact ring graben on Europa. In: 37th Annual Lunar and Planetary Science Conference, p 2399. https://www.lpi.usra.edu/meetings/lpsc2006/pdf/2399.pdf

Manga M, Michaut C (2017) Formation of lenticulae on Europa by saucer-shaped sills. Icarus 286:261–269. https://doi.org/10.1016/j.icarus.2016.10.009

Manga M, Sinton A (2004) Formation of bands and ridges on Europa by cyclic deformation: insights from analogue wax experiments. J Geophys Res, Planets 1991(2012):109. https://doi.org/10.1029/2004JE002249

Mazarico E, Buccino D, Castillo-Rogez J et al (2023) The Europa clipper gravity and radio science investigation. Space Sci Rev 219:30. https://doi.org/10.1007/s11214-023-00972-0

McEwen AS (1986) Exogenic and endogenic albedo and color patterns on Europa. J Geophys Res, Solid Earth 91(B8):8077–8097

McEwen AS, Keszthelyi L, Geissler P, Simonelli DP, Carr MH et al (1998) Active volcanism on Io as seen by Galileo SSI. Icarus 135:181–219. https://doi.org/10.1006/icar.1998.5972

Meitzler R, Jun I, Blase R et al (2023) Investigating Europa's radiation environment with the Europa Clipper radiation monitor. Space Sci Rev 219:61. https://doi.org/10.1007/s11214-023-01003-8

Melosh HJ, Turtle EP (2004) Ridges on Europa: origin by incremental ice-wedging. In: Proceedings of the lunar and planetary science conference XXXV. Abstract 2029

Michaelides RJ, Schroeder D (2019) Doppler-based discrimination of radar sounder target scattering properties: a case study of subsurface water geometry in Europa's ice shell. Icarus 326:29–36. https://doi.org/10.1016/j.icarus.2019.02.037

Michaut C, Manga M (2014) Domes, pits, and small chaos on Europa produced by water sills. J Geophys Res, Planets 119(3):550–573. https://doi.org/10.1002/2013JE004558

Mitri G, Showman AP (2005) Convective conductive transitions and sensitivity of a convecting ice shell to perturbations in heat flux and tidal-heating rate: implications for Europa. Icarus 177:447–460. https://doi.org/10.1016/j.icarus.2005.03.019

Molaro JL, Meirion-Griffith G, Phillips CB, Mitchell KL, Hodyss R, Choukroun M (2018) Microstructural evolution of solar system ices through sintering. In: 49th Annual Lunar and Planetary Science Conference, p 2977. https://www.hou.usra.edu/meetings/lpsc2018/pdf/2977.pdf

Moore JM, Asphaug E, Sullivan RJ, Klemaszewski JE, Bender KC, Greeley R, Geissler PE, McEwen AS, Turtle EP, Phillips CB, Tufts BR, Head JW, Pappalardo RT, Jones KB, Chapman CR, Belton MJS, Kirk RL, Morrison D (1998) Large impact features on Europa: results of the Galileo nominal mission. Icarus 135:127–145. https://doi.org/10.1006/icar.1998.5973

Moore JM, Asphaug E, Morrison D, Klemaszewski JE, Sullivan RJ et al (1999) Mass movement and landform degradation on the icy Galilean satellites: results from the Galileo nominal mission. Icarus 140:294–312

Moore JM, et al (2001) Impact features on Europa: results of the Galileo Europa mission (GEM). Icarus 151:93–111.

Moore JM, Black G, Buratti B, Phillips CB, Spencer J, Sullivan R (2009) Surface properties, regolith, and landscape degradation. In: Pappalardo RT, McKinnon WB, Khurana KK (eds) Europa. University of Arizona Press, Tucson, pp 329–349

National Research Council (2003) New frontiers in the solar system: an integrated exploration strategy. The National Academies Press, Washington. https://doi.org/10.17226/10432

National Research Council (2011) Vision and voyages for planetary science in the decade 2013-2022. The National Academies Press, Washington. https://doi.org/10.17226/13117

National Academies of Sciences, Engineering, and Medicine (2022) Origins, Worlds, and Life: A Decadal Strategy for Planetary Science and Astrobiology 2023–2032. The National Academies Press, Washington. https://doi.org/10.17226/26522

Neish CD, Prockter LM, Patterson GW (2012) Observational constraints on the identification and distribution of chaotic terrain on icy satellites. Icarus 221(1):72–79. https://doi.org/10.1016/j.icarus.2012.07.009

Nelessen A et al (2019) Mars 2020 entry, descent, and landing system overview. In: 2019 IEEE aerospace conference, pp 1–20. https://doi.org/10.1109/AERO.2019.8742167

Nimmo F, Gaidos E (2002) Strike-slip motion and double ridge formation on Europa. J Geophys Res, Planets 107(E4):5-1

Nimmo F, Giese B, Pappalardo RT (2003) Estimates of Europa's ice shell thickness from elastically-supported topography. Geophysical Research Letters 30:1233. https://doi.org/10.1029/2002GL016660

Nordheim T, Hand K, Paranicas C (2018) Preservation of potential biosignatures in the shallow subsurface of Europa. Nat Astron 2:673–679. https://doi.org/10.1038/s41550-018-0499-8

Noviello JL, Torrano ZA, Rhoden AR, Singer KN (2019) Mapping Europa's microfeatures in regional mosaics: new constraints on formation models. Icarus 329:101–123. https://doi.org/10.1016/j.icarus.2019.02.038

Nuñez KA et al (2019) Developing a Database for Candidate Cryovolcanic Domes on Europa 50th Lunar and Planetary Science Conference. 2019 (LPI Contrib. No. 2132) Abstract No. 3264

O'Brien D (2002) A melt-through model for chaos formation on Europa. Icarus 156(1):152–161. https://doi.org/10.1006/icar.2001.6777

Ojakangas GW, Stevenson DJ (1986) Episodic volcanism of tidally heated satellites with application to Io. Icarus 66(2):341–358

Ostro SJ, Shoemaker EM (1990) The extraordinary radar echoes from Europa, Ganymede, and Callisto: a geological perspective. Icarus 85:335–345. https://doi.org/10.1016/0019-1035(90)90121-O

Paganini L, Villanueva GL, Roth L, Mandell AM, Hurford TA, Retherford KD, Mumma MJ (2020) A measurement of water vapour amid a largely quiescent environment on Europa. Nat Astron 4:266–272

Pappalardo RT, Barr AC (2004) The origin of domes on Europa: the role of thermally induced compositional diapirism. Geophys Res Lett 31(1):L01701. https://doi.org/10.1029/2003GL019202

Pappalardo R, Coon MD (1996) A sea ice analog for the surface of Europa. In: 27th Lunar and planetary science conference, p 997

Pappalardo RT, Sullivan RJ (1996) Evidence for separation across a gray band on Europa. Icarus 123(2):557–567

Pappalardo RT, Head JW, Greeley R, Sullivan RJ, Pilcher C, Schubert G, Moore WB, Carr MH, Moore JM, Belton MJS, Goldsby DL (1998a) Geological evidence for solid-state convection in Europa's ice shell. Nature 391:365–368

Pappalardo RT, Head JW, Sherman ND, Greeley R, Sullivan RJ (1998b) Classification of Europan ridges and troughs and a possible genetic sequence. In: Proceedings of the lunar and planetary science conference XXIX. Abstract 1859

Pappalardo RT, Belton MJS, Breneman HH, Carr MH, Chapman CR, Collins GC, Denk T, Fagents S, Geissler PE, Giese B, Greeley R, Greenberg R, Head JW, Helfenstein P, Hoppa G, Kadel SD, Klaasen KP, Klemaszewski JE, Magee K, McEwen AS, Moore JM, Moore WB, Neukum G, Phillips CB, Prockter LM, Schubert G, Senske DA, Sullivan RJ, Tufts BR, Turtle EP, Wagner R, Williams KK (1999) Does Europa have a subsurface ocean? Evaluation of the geological evidence. J Geophys Res 104:24015–24055

Pappalardo RT et al (2024) Science overview of the Europa Clipper Mission. Space Sci Rev 220

Paranicas C, Carlson RW, Johnson RE (2001) Electron bombardment of Europa. Geophys Res Lett 28:673–676

Paranicas C, Mitchell DG, Krimigis SM, Carbary JF, Brandt PC, Turner FS, Roussos E, Krupp N, Kivelson MG, Khurana KK, Cooper JF, Armstrong TP, Burton M (2010) Asymmetries in Saturn's radiation belts. Journal of Geophysical Research (Space Physics) 115:A07216. https://doi.org/10.1029/2009JA014971

Parekh R, Pappalardo R, Scully JEC (2023) Small-scale mass movements on Europa, Callisto & Ganymede. In: 54th Lunar and Planetary Science Conference, LPI Contribution No 2806, id 1876

Patterson GW, Prockter LM, Schenk PM (2010) Insights into the formation and evolution of Europa's bands from relationships involving morphology, topography, and relative age. In: European Planetary Science Congress 2010, 828. https://ui.adsabs.harvard.edu/abs/2010epsc.conf..828P/abstract

Phillips CB (2015) Searching for plumes and ongoing geologic activity on Europa. LPSC 46:#2704

Phillips C, Korth H (2017) Choice of coordinate systems for planetary mapping by the Europa clipper project. Available online at https://sbn.psi.edu/mc-f2f/2017/presentations/Europa%20Clipper%20Coordinate%20System%20Convention%2020170803.pdf

Phillips CB, McEwen AS, Hoppa GV, Fagents SA, Greeley R, Klemaszewski JE, Pappalardo RT, Klaasen KP, Breneman HH (2000) The search for current geologic activity on Europa. J Geophys Res, Planets 105(E9):22579–222597. https://doi.org/10.1029/1999JE001139

Phillips CB et al (2020) An exploration strategy for Europa. Planetary science and astrobiology decadal survey, white paper

Phillips CB et al (2023) A Reconnaissance Strategy for Landing on Europa. Based on Europa Clipper Data. Submitted

Pike R (1980) Control of crater morphology by gravity and target type: Mars, Earth, Moon. Proc Lunar Planet Sci Conf 11:2159–2189

Prieto-Ballesteros O, Kargel JS, Fernández-Sampedro M, Selsis F, Martínez ES, Hogenboom DL (2005) Evaluation of the possible presence of clathrate hydrates in Europa's icy shell or seafloor. Icarus 177(2):491–505

Prockter LM, Pappalardo RT (2000) Folds on Europa: implications for crustal cycling and accommodation of extension. Science 289(5481):941–943

Prockter LM, Patterson GW (2009) Morphology and evolution of Europa's ridges and bands. In: Pappalardo RT, McKinnon WB, Khurana KK (eds) Europa. University of Arizona Press, Tucson, pp 237–258

Prockter L, Schenk P (2005) Origin and evolution of castalia macula: an anomalous young depression on Europa. Icarus 177:305–326

Prockter LM, Schenk PM (2016) The geological context and history of Thrace Macula, Europa. In: 47th Annual Lunar and Planetary Science Conference, p 1673. https://www.hou.usra.edu/meetings/lpsc2016/pdf/1673.pdf

Prockter LM, Antman AM, Pappalardo RT, Head JW, Collins GC (1999) Europa: stratigraphy and geological history of the anti-Jovian region from Galileo E14 solid-state imaging data. J Geophys Res, Planets 104:16531–16540

Prockter LM, Figueredo PH, Pappalardo RT, Head JW, Collins GC (2000) Geology and mapping of dark terrain on Ganymede and implications for grooved terrain formation. J Geophys Res, Planets 105:22519–22540

Prockter LM, Head JW III, Pappalardo RT, Sullivan RJ, Clifton AE, Giese B et al (2002) Morphology of Europan bands at high resolution: a mid-ocean ridge-type rift mechanism. J Geophys Res, Planets 107(E5):4-1

Prockter LM, Shirley JH, Dalton JB III, Kamp L (2017) Surface composition of pull-apart bands in Argadnel Regio, Europa: evidence of localized cryovolcanic resurfacing during basin formation. Icarus 285:27–42

Quick LC, Hedman MM (2020) Characterizing surface deposits emplaced by cryovolcanic plumes on Europa. Icarus 343:113667. https://doi.org/10.1016/j.icarus.2020.113667

Quick LC, Marsh BD (2016) Heat transfer and cooling of ascending cryomagmas on Europa. J Volcanol Geotherm Res 319:66–77

Quick LC, Barnouin OS, Patterson GW, Prockter LM (2010) Constraints on the detection of cryovolcanic plumes on Europa. In: 41st Lunar and Planetary Science Conference. Abstract #2247

Quick LC, Barnouin OS, Prockter LM, Patterson GW (2013) Constraints on the detection of cryovolcanic plumes on Europa. Planet Space Sci 86:1–9

Quick LC, Glaze LS, Baloga SM (2017) Cryovolcanic emplacement of domes on Europa. Icarus 284:477–488

Quick LC et al (2019) A possible brine reservoir beneath occator crater: thermal and compositional evolution and formation of the Cerealia Dome and Vinalia Faculae. Icarus 320:119–135. https://doi.org/10.1016/j.icarus.2018.07.016

Quick LC et al (2021) A volume flux approach to Europa Cryolava Dome formation and implications for the thermal evolution of crustal fluid reservoirs 52nd Lunar and Planetary Science Conference LPI Contribution. No. 2548, Abstract No. 2637

Quick LC et al (2022) Cryolava dome growth resulting from active eruptions on Jupiter's moon Europa. Icarus 387:115185. https://doi.org/10.1016/j.icarus.2022.115185

Rathbun JA, Spencer JR (2020) Proposed plume source regions on Europa: no evidence for endogenic thermal emission. Icarus 338:113500. https://doi.org/10.1016/j.icarus.2019.113500

Rathbun JA, Musser GS, Squyres SW (1998) Ice diapirs on Europa: implications for liquid water. Geophys Res Lett 25(22):4157–4160. https://doi.org/10.1029/1998GL900135

Rathbun JA, Rodriguez NJ, Spencer JR (2010) Galileo PPR observations of Europa: hotspot detection limits and surface thermal properties. Icarus 210:763–769. https://doi.org/10.1016/j.icarus.2010.07.017

Rathbun JA, Spencer JR, Tamppari LK, Martin TZ, Barnard L, Travis LD (2004) Mapping of Io's thermal radiation by the Galileo photopolarimeter-radiometer (PPR) instrument. Icarus 169:127–139. https://doi.org/10.1016/j.icarus.2003.12.021

Rathbun JA, Spencer JR, Lopes RM, Howell RR (2014) Io's active volcanoes during the New Horizons era: insights from New Horizons imaging. Icarus 231:261–272. https://doi.org/10.1016/j.icarus.2013.12.002

Rhoden AR, Militzer B, Huff EM, Hurford TA, Manga M, Richards MA (2010) Constraints on Europa's rotational dynamics from modeling of tidally-driven fractures. Icarus 210(2):770–784

Rhoden AR, Hurford TA, Roth L, Retherford K (2015) Linking Europa's plume activity to tides, tectonics, and liquid water. Icarus 253:169–178

Rhoden AR, Mohr KJ, Hurford TA, Henning W, Sajous S, Patthoff DA, Dubois D (2021) Obliquity, precession, and fracture mechanics: Implications of Europa's global cycloid population. J Geophys Res, Planets e2020JE006710

Robbins SJ, Watters WA, Chappelow JE, Bray VJ, Daubar IJ, Craddock RA, Beyer RA, Landis ME, Ostrach LR, Tornabene LL, Riggs JD, Weaver BP (2017) Measuring impact crater depth throughout the solar system. Meteorit Planet Sci 44:1–44. https://doi.org/10.1111/maps.12956

Roberts JH, McKinnon WB, Elder CM et al (2023) Exploring the interior of Europa with the Europa Clipper. Space Sci Rev 219:46. https://doi.org/10.1007/s11214-023-00990-y

Roth L, Retherford KD, Saur J, Strobel DF, Feldman PD, McGrath MA, Nimmo F (2014b) Orbital apocenter is not a sufficient condition for HST/STIS detection of Europa's water vapor aurora. Proc Natl Acad Sci 111:E5123–E5132

Roth L, Saur J, Retherford KD, Strobel DF, Feldman PD, McGrath MA, Nimmo F (2014a) Transient water vapor at Europa's south pole. Science 343:171–174

Roth L, Retherford KD, Ivchenko N, Schlatter N, Strobel DF, Becker TM, Grava C (2017) Detection of a hydrogen corona in HST Lyα images of Europa in transit of Jupiter. Astron J 153:67. https://doi.org/10.3847/1538-3881/153/2/67

Sarid AR, Hurford TA, Manga M (2009) Strike-slip on Europa-the faults of polar wander or obliquity?. In: AAS/division for planetary sciences meeting, Abstracts# 41, pp 66-07

Scanlan KM, Grima C, Steinbrügge G, Kempf SD, Young DA, Blankenship DD (2019) Geometric determination of ionosphere total electron content from dual frequency radar sounding measurements. Planet Space Sci 178:104696. https://doi.org/10.1016/j.pss.2019.07.010

Schenk P, McKinnon WB, Moore J, Nimmo F (2021) The topography of Ganymede (and Callisto): geology, global characteristics, and future exploration. In: 52nd Lunar and Planetary Science Conference, p 2228

Schenk PM (2002) Thickness constraints on the icy shells of the Galilean satellites from a comparison of crater shapes. Nature 417:419–421. https://doi.org/10.1038/417419a

Schenk PM (2009) Slope characteristics of Europa: constraints for landers and radar sounding. Geophysical Research Letters 36:L15204. https://doi.org/10.1029/2009GL039062

Schenk P (2010) Atlas of the Galilean satellites. Cambridge University Press, Cambridge. https://doi.org/10.1017/CBO9780511676468

Schenk PM (2020) The search for Europa's plumes: no surface patterns or changes 1979–2007? Astrophys J Lett 89:L12

Schenk PM, McKinnon WB (1989) Fault offsets and lateral crustal movement on Europa: evidence for a mobile ice shell. Icarus 79(1):75–100

Schenk PM, McKinnon WB (2001) Topographic variability on Europa from Galileo stereo images. In: Proceedings of lunar and planetary science conference, vol 32, p. 2078

Schenk PM, Pappalardo RT (2004) Topographic variations in chaos on Europa: Implications for diapiric formation. Geophys Res Lett 31(16). https://doi.org/10.1029/2004GL019978

Schenk PM, Turtle EP (2009) Europa's impact craters: probes of the icy shell. In: Pappalardo RT, McKinnon WB, Khurana KK (eds) Europa. University of Arizona Press, Tucson, pp 181–198

Schenk PM, Chapman CR, Zahnle K, Moore JM (2004) Ages and interiors: the cratering record of the Galilean satellites. In: Bagenal F, Dowling TE, McKinnon WB (eds) Jupiter. The planet, satellites and magnetosphere. Cambridge University Press, pp 427–456

Schenk P, Matsuyama I, Nimmo F (2008) True polar wander on Europa from global-scale small-circle depressions. Nature 453(7193):368–371. https://doi.org/10.1038/nature06911

Schenk P, Matsuyama I, Nimmo F (2020) A very young age for true polar wander on Europa from related fracturing. Geophys Res Lett 47(17):e2020GL088364

Schmidt BE, Blankenship DD, Patterson GW, Schenk PM (2011) Active formation of 'chaos terrain' over shallow subsurface water on Europa. Nature 479(7374):502–505. https://doi.org/10.1038/nature10608

Shirley JH et al (2010) Europa's ridged plains and smooth low albedo plains: distinctive compositions and compositional gradients at the leading side–trailing side boundary. Icarus 210(1):358–384

Shirley JH, Dalton JB, Kamp LW (2011) Surface Composition of Europa's Icy Bright Plains and Dark Linea: Leading side versus trailing side comparisons p 1201. EPSC-DPS Joint Meeting, 2011

Showman AP, Han L (2005) Effects of plasticity on convection in an ice shell: implications for Europa. Icarus 177(2):425–437. https://doi.org/10.1016/j.icarus.2005.02.020

Singer KN, McKinnon WB, Schenk PM (2013) Ice lithosphere thickness on Europa from impact basin ring-graben. In: Lunar and planetary science conference, Abstract 2197

Singer KN, McKinnon WB, Schenk PM (2021) Pits, uplifts and small chaos features on Europa: morphologic and morphometric evidence for intrusive upwelling and lower limits to ice shell thickness. Icarus 364:114465. https://doi.org/10.1016/j.icarus.2021.114465

Skjetne HL, Singer KN, Hynek BM, Knight KI, Schenk PM, Olkin CB, White OL, Bertrand T, Runyon KD, McKinnon WB, Moore JM, Stern SA, Weaver HA, Young LA, Ennico K (2021) Morphological comparison of blocks in chaos terrains on Pluto, Europa, and Mars. Icarus 356:113866. https://doi.org/10.1016/j.icarus.2020.113866

Sotin C, Head JW III, Tobie G (2002) Europa: tidal heating of upwelling thermal plumes and the origin of lenticulae and chaos melting. Geophys Res Lett 29(8):74-1

Sparks WB, Hand KP, McGrath MA, Bergeron E, Cracraft M, Deustua SE (2016) Probing for evidence of plumes on Europa with HST/STIS. Astrophys J 829:121

Sparks WB, Schmidt BE, McGrath MA, Hand KP, Spencer JR, Cracraft M, Deustua SE (2017) Active cryo-volcanism on Europa? Astrophys J Lett 839(2):L18

Sparks WB, Richter M, deWitt C, Montiel E, Dello Russo N et al (2019) A search for water vapor plumes on Europa using SOFIA. Astrophys J Lett 871:L5. https://doi.org/10.3847/2041-8213/aafb0a

Spaun NA, Head JW, Collins GC, Prockter LM, Pappalardo RT (1998) Conamara chaos region, Europa: reconstruction of mobile polygonal ice blocks. Geophys Res Lett 25(23):4277–4280. https://doi.org/10.1029/1998GL900176

Spaun NA, Head JW, Pappalardo RT (1999) Chaos and lenticulae on Europa: structure, morphology and comparative analysis. Presented at the 30th lunar and planetary science conference

Spencer JR (1987) The surfaces of Europa, Ganymede, and Callisto: an investigation using Voyager IRIS thermal infrared spectra. Ph.D. Dissertation, University of Arizona

Spencer JR, Tamppari LK, Martin TZ, Travis LD (1999) Temperatures on Europa from Galileo photopolarimeter-radiometer: nighttime thermal anomalies. Science 284:1514–1516. https://doi.org/10.1126/science.284.5419.1514

Spencer JR et al (2006) Cassini encounters Enceladus: background and the discovery of a south polar hot spot. Science 311(5766):1401–1405. https://doi.org/10.1126/science.1121661

Steinbrügge G, Voight JRC, Wolfenbarger NS, Hamilton CW, Soderlund KM, Young DA, Blankenship DD, Vance SD, Schroeder DM (2020a) Brine migration and impact-induced Cryovolcanism on Europa. Geophys Res Lett 47:e2020GL090797

Steinbrügge G, Voigt JRC, Schroeder DM, Stark A, Haynes MS, Scanlan KM et al (2020b) The surface roughness of Europa derived from Galileo stereo images. Icarus 343:113669. https://doi.org/10.1016/j.icarus.2020.113669

Stempel MM, Barr AC, Pappalardo RT (2005) Model constraints on the opening rates of bands on Europa. Icarus 177(2):297–304. https://doi.org/10.1016/j.icarus.2005.03.025

Sullivan R, Greeley R, Homan K, Klemaszewski J, Belton MJS, Carr MH, Chapman CR, Tufts R, Head JW, Pappalardo R, Moore J, Thomas P (1998) Episodic plate separation and fracture infill on the surface of Europa. Lett Nat 391:371–373

Sullivan R, Moore J, Pappalardo R (1999) Mass-wasting and slope evolution on Europa. LPSC 30:#1747

Teolis BD, Wyrick DY, Bouquet A, Magee BA, Waite JH (2017) Plume and surface feature structure and compositional effects on Europa's global exosphere: preliminary Europa mission predictions. Icarus 284:18–29

Trumbo SK, Brown ME, Butler BJ (2018) ALMA thermal observations of Europa. Astron J 156:161. https://doi.org/10.3847/1538-3881/aada87

Tufts BR, Greenberg R, Hoppa G, Geissler P (2000) Lithospheric dilation on Europa. Icarus 146:75–97

Turtle EP (1998) Finite-element modeling of large impact craters: Implications for the size of the Vredefort structure and the formation of multiple ring craters. Ph.D. Thesis, University of Arizona

Turtle EP, Pierazzo E (2001) Thickness of a Europan ice shell from impact crater simulations. Science 294(5545):1326–1328

Turtle EP, Melosh HJ, Phillips CB (1998) Europan ridges: tectonic response to dike intrusion. Eos Trans AGU 79(17):S202

Vance SD, Craft KL, Shock E et al (2023) Investigating Europa's habitability with the Europa Clipper. Space Sci Rev 219:81. https://doi.org/10.1007/s11214-023-01025-2

Waite Jr JH et al (2024) MASPEX-Europa: the Europa Clipper neutral gas mass spectrometer investigation. Space Sci Rev 220

Walker CC, Schmidt BE (2018) Investigating active chaos formation as the source of Europa's water vapor plumes. In: 49th Lunar and Planetary Science Conference. Abstract #1302

Westlake JH, McNutt RL, Grey M et al (2023) The Plasma Instrument for Magnetic Sounding (PIMS) on the Europa Clipper Mission. Space Sci Rev 219:62. https://doi.org/10.1007/s11214-023-01002-9

Williams KK, Greeley R (1998) Estimates of ice thickness in the Conamara Chaos Region of Europa. Geophys Res Lett 25(23):4273–4276. https://doi.org/10.1029/1998GL900144

Wilson L, Head JW, Pappalardo RT (1997) Eruption of lava flows on Europa: theory and application to Thrace Macula. J Geophys Res, Planets 102(E4):9263–9272

Zahnle K, Schenk P, Levison H, Dones L (2003) Cratering rates in the outer solar system. Icarus 163(2):263–289

Zahnle K, Alvarellos JL, Dobrovolskis A, Hamill P (2008) Secondary and sesquinary craters on Europa. Icarus 194(2):660–674

Authors and Affiliations

I.J. Daubar[1,2] · **A.G. Hayes[3]** · **G.C. Collins[4]** · **K.L. Craft[5]** · **J.A. Rathbun[3]** · **J.R. Spencer[6]** · **D.Y. Wyrick[7]** · **M.T. Bland[8]** · **A.G. Davies[1]** · **C.M. Ernst[5]** · **S.M. Howell[1]** · **E.J. Leonard[1]** ·

**A.S. McEwen[9] · J.M. Moore[10] · C.B. Phillips[1] · L.M. Prockter[5] · L.C. Quick[11] · J.E.C. Scully[1] ·
J.M. Soderblom[12] · S.M. Brooks[1] · M. Cable[1] · M.E. Cameron[1] · K. Chan[13] · C.J. Chivers[14] ·
M. Choukroun[1] · C.J. Cochrane[1] · S. Diniega[1] · A.J. Dombard[15] · C.M. Elder[1] ·
C. Gerekos[16] · C. Glein[7] · T.K. Greathouse[7] · C. Grima[13] · M.S. Gudipati[1] · K.P. Hand[1] ·
C. Hansen[17] · P. Hayne[18] · M. Hedman[19] · K. Hughson[20] · X. Jia[21] · J. Lawrence[22] ·
H.M. Meyer[5] · K. Miller[7] · R. Parekh[1] · G.W. Patterson[5] · D.M. Persaud[23] · S. Piqueux[1] ·
K.D. Retherford[7,24] · K.M. Scanlan[13] · P. Schenk[17] · B. Schmidt[25] · D. Schroeder[26] ·
G. Steinbrügge[1] · A. Stern[6] · G. Tobie[27] · P. Withers[28] · D.A. Young[13] · B. Buratti[1] ·
H. Korth[5] · D. Senske[1] · R. Pappalardo[1]**

✉ I.J. Daubar
   ingrid.daubar@jpl.nasa.gov

   A.G. Hayes
   hayes@astro.cornell.edu

   G.C. Collins
   gcollins@wheatonma.edu

   K.L. Craft
   Kate.Craft@jhuapl.edu

   J.A. Rathbun
   rathbun@psi.edu

   J.R. Spencer
   spencer@boulder.swri.edu

   D.Y. Wyrick
   dwyrick@swri.org

   M.T. Bland
   mbland@usgs.gov

   A.G. Davies
   ashley.davies@jpl.nasa.gov

   C.M. Ernst
   carolyn.ernst@jhuapl.edu

   S.M. Howell
   samuel.m.howell@jpl.nasa.gov

   E.J. Leonard
   erin.j.leonard@jpl.nasa.gov

   A.S. McEwen
   mcewen@lpl.arizona.edu

   J.M. Moore
   jeff.moore@nasa.gov

   C.B. Phillips
   Cynthia.B.Phillips@jpl.nasa.gov

   L.M. Prockter
   louise.prockter@jhuapl.edu

   L.C. Quick
   Lynnae.C.Quick@nasa.gov

   J.E.C. Scully
   jennifer.e.scully@jpl.nasa.gov

   J.M. Soderblom
   jms4@mit.edu

S.M. Brooks
Shawn.M.Brooks@jpl.nasa.gov

M. Cable
morgan.l.cable@jpl.nasa.gov

M.E. Cameron
marissa.e.cameron@jpl.nasa.gov

K. Chan
kristian.chan@utexas.edu

C.J. Chivers
chase.chivers@whoi.edu

M. Choukroun
Mathieu.Choukroun@jpl.nasa.gov

C.J. Cochrane
Corey.J.Cochrane@jpl.nasa.gov

S. Diniega
Serina.Diniega@jpl.nasa.gov

A.J. Dombard
adombard@uic.edu

C.M. Elder
Catherine.Elder@jpl.nasa.gov

C. Gerekos
christopher.gerekos@austin.utexas.edu

C. Glein
cglein@swri.edu

T.K. Greathouse
tgreathouse@swri.edu

C. Grima
cyril.grima@utexas.edu

M.S. Gudipati
Murthy.Gudipati@jpl.nasa.gov

K.P. Hand
Kevin.P.Hand@jpl.nasa.gov

C. Hansen
cjhansen@psi.edu

P. Hayne
Paul.Hayne@lasp.colorado.edu

M. Hedman
mhedman@uidaho.edu

K. Hughson
kynan.hughson@unb.ca

X. Jia
xzjia@umich.edu

J. Lawrence
jdlawrence@honeybeerobotics.com

H.M. Meyer
Heather.Meyer@jhuapl.edu

K. Miller
Kmiller@swri.edu

R. Parekh
rutu.a.parekh@jpl.nasa.gov

G.W. Patterson
Gerald.Patterson@jhuapl.edu

D.M. Persaud
divya.persaud@glasgow.ac.uk

S. Piqueux
Sylvain.Piqueux@jpl.nasa.gov

K.D. Retherford
KRetherford@swri.edu

K.M. Scanlan
kimis@dtu.dk

P. Schenk
schenk@lpi.usra.edu

B. Schmidt
britneys@cornell.edu

D. Schroeder
Dustin.M.Schroeder@stanford.edu

G. Steinbrügge
gregor.b.steinbruegge@jpl.nasa.gov

A. Stern
alan@boulder.swri.edu

G. Tobie
Gabriel.Tobie@univ-nantes.fr

P. Withers
withers@bu.edu

D.A. Young
duncan@ig.utexas.edu

B. Buratti
Bonnie.Buratti@jpl.nasa.gov

H. Korth
haje.korth@jhuapl.edu

D. Senske
Dsenske1924@gmail.com

R. Pappalardo
robert.pappalardo@jpl.nasa.gov

1   California Institute of Technology, Pasadena, CA, USA

2   Brown University, Providence, RI, USA

3   Cornell University, Ithaca, NY, USA

4   Wheaton College, Norton, MA, USA

5   Johns Hopkins University Applied Physics Laboratory, Laurel, MD, USA

6   Southwest Research Institute, Boulder, CO, USA

7   Southwest Research Institute, San Antonio, TX, USA

8   United States Geological Survey, Flagstaff, AZ, USA

[9]   University of Arizona, Tucson, AZ, USA

[10]   NASA-Ames, Mountain View, CA, USA

[11]   NASA Goddard Space Flight Center, Greenbelt, MD, USA

[12]   Massachusetts Institute of Technology, Cambridge, MA, USA

[13]   University of Texas Institute for Geophysics, Austin, TX, USA

[14]   Woods Hole Oceanographic Institution, Woods Hole, MA, USA

[15]   University of Illinois Chicago, Chicago, IL, USA

[16]   University of Texas Austin, Austin, TX, USA

[17]   Planetary Science Institute, Tucson, AZ, USA

[18]   University of Colorado, Boulder, CO, USA

[19]   University of Idaho, Moscow, ID, USA

[20]   Georgia Institute of Technology, Atlanta, GA, USA

[21]   University of Michigan, Ann Arbor, MI, USA

[22]   Honeybee Robotics, Altadena, CA, USA

[23]   University of Glasgow, Glasgow, UK

[24]   University of Texas at San Antonio, San Antonio, TX, USA

[25]   Dept of Astronomy and Earth & Atmospheric Sciences, Cornell University, Ithaca, NY, USA

[26]   Stanford University, Stanford, CA, USA

[27]   Laboratory of Planetology and Geosciences, Nantes University, Nantes, France

[28]   Boston University, Boston, MA, USA